AGU PUBLICATIONS

Paleoceanography

RESEARCH ARTICLE
10.1002/2014PA002763

Key Points:
- Subarctic Pacific surface hydrography and nutrient utilization are reconstructed
- Late Heinrich 1 sea ice-related paleoceanographic change in subarctic Pacific
- Subarctic Pacific CO_2 degassing from late Heinrich 1 to Younger Dryas

Supporting Information:
- Figures S1–S5 and Tables S1–S5

Correspondence to:
E. Maier,
edith.maier@awi.de

Citation:
Maier, E., M. Méheust, A. Abelmann, R. Gersonde, B. Chapligin, J. Ren, R. Stein, H. Meyer, and R. Tiedemann (2015), Deglacial subarctic Pacific surface water hydrography and nutrient dynamics and links to North Atlantic climate variability and atmospheric CO_2, *Paleoceanography*, *30*, 949–968, doi:10.1002/2014PA002763.

Received 26 NOV 2014
Accepted 21 JUN 2015
Accepted article online 24 JUN 2015
Published online 23 JUL 2015
Corrected 19 AUG 2015

This article was corrected on 19 AUG 2015. See the end of the full text for details.

Deglacial subarctic Pacific surface water hydrography and nutrient dynamics and links to North Atlantic climate variability and atmospheric CO_2

E. Maier[1], M. Méheust[1], A. Abelmann[1], R. Gersonde[1], B. Chapligin[2], J. Ren[1], R. Stein[1], H. Meyer[2], and R. Tiedemann[1]

[1]Alfred Wegener Institute Helmholtz Centre for Polar and Marine Research, Bremerhaven, Germany, [2]Alfred Wegener Institute Helmholtz Centre for Polar and Marine Research, Potsdam, Germany

Abstract The glacial-to-Holocene evolution of subarctic Pacific surface water stratification and silicic acid (Si) dynamics is investigated based on new combined diatom oxygen ($\delta^{18}O_{diat}$) and silicon ($\delta^{30}Si_{diat}$) isotope records, along with new biogenic opal, subsurface foraminiferal $\delta^{18}O$, alkenone-based sea surface temperature, sea ice, diatom, and core logging data from the NE Pacific. Our results suggest that $\delta^{18}O_{diat}$ values are primarily influenced by changes in freshwater discharge from the Cordilleran Ice Sheet (CIS), while corresponding $\delta^{30}Si_{diat}$ are primarily influenced by changes in Si supply to surface waters. Our data indicate enhanced glacial to mid Heinrich Stadial 1 (HS1) NE Pacific surface water stratification, generally limiting the Si supply to surface waters. However, we suggest that an increase in Si supply during early HS1, when surface waters were still stratified, is linked to increased North Pacific Intermediate Water formation. The coincidence between fresh surface waters during HS1 and enhanced ice-rafted debris sedimentation in the North Atlantic indicates a close link between CIS and Laurentide Ice Sheet dynamics and a dominant atmospheric control on CIS deglaciation. The Bølling/Allerød (B/A) is characterized by destratification in the subarctic Pacific and an increased supply of saline, Si-rich waters to surface waters. This change toward increased convection occurred prior to the Bølling warming and is likely triggered by a switch to sea ice-free conditions during late HS1. Our results furthermore indicate a decreased efficiency of the biological pump during late HS1 and the B/A (possibly also the Younger Dryas), suggesting that the subarctic Pacific has then been a source region of atmospheric CO_2.

1. Introduction

Deglacial variations in thermohaline overturning circulation are thought to have played a key role in changing atmospheric CO_2 concentrations via changes in upper ocean stratification in high latitudes [*Sigman et al.*, 2010]. Deglacial destratification especially in the Southern Ocean may have provided a pathway for CO_2 exchange between the deep ocean and the atmosphere during Heinrich Stadial 1 (HS1) [*Skinner et al.*, 2010; *Burke and Robinson*, 2012], thereby increasing atmospheric CO_2 concentrations as recorded in ice cores [*Schmitt et al.*, 2012; *Parrenin et al.*, 2013; *Marcott et al.*, 2014]. During the past decade the subarctic Pacific received increased paleoceanographic attention with the aim to examine its potential for influencing the nutrient cycle and the oceanic release of CO_2 via deep/intermediate water formation, upwelling, and associated changes in biogenic productivity [e.g., *Galbraith et al.*, 2007; *Lam et al.*, 2013; *Rae et al.*, 2014]. Today, the subarctic Pacific is considered a weak sink for CO_2 [*Lefèvre et al.*, 1999; *Ayers and Lozier*, 2012], despite regions of incomplete nutrient utilization (Figure 1a). Accordingly, changes in subarctic Pacific upper ocean stratification and/or biological nutrient utilization and export production have the potential to effectively influence the oceanic-atmospheric gas exchange.

Today, the subarctic Pacific is characterized by a steep salinity stratification, with the low-salinity surface waters sustained by a large freshwater flux and relatively small regional evaporation [*Warren*, 1983; *Broecker et al.*, 1990; *Emile-Geay et al.*, 2003]. As a consequence of the halocline there is only limited vertical exchange between surface waters and deeper, nutrient- and CO_2-rich waters. However, these conditions may have been different during HS1. Recent studies provide evidence for increased ventiliation of North Pacific intermediate waters [*Jaccard*, 2012; *Jaccard and Galbraith*, 2013; *Max et al.*, 2014] or even

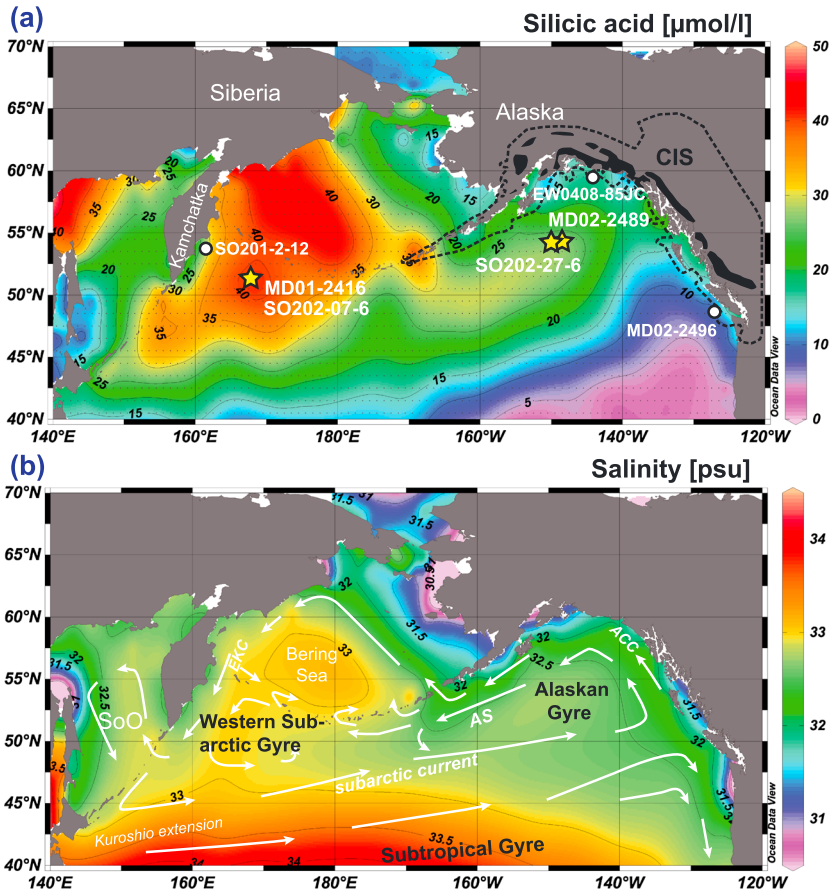

Figure 1. (a) Mean annual silicic acid concentration of subarctic Pacific surface waters [*Garcia et al.*, 2010], distribution of modern glaciers in the North American Cordillera (black areas), maximum extent of the Cordilleran Ice Sheet (CIS) during the last glacial (black dashed contour) [after *Clague and James*, 2002; *Kaufman et al.*, 2011], as well as core sites of this study (yellow stars) and of other cores mentioned in the text (white circles). (b) Mean annual sea surface salinity [*Antonov et al.*, 2010] as well as surface water currents [after *Dodimead et al.*, 1963; *Stabeno et al.*, 2004]: ACC: Alaska Coastal Current; AS: Alaskan Stream; EKC: East Kamchatka Current; and SoO: Sea of Okhotsk. The maps were created with Ocean Data View (www.odv.awi.de).

suggest deep convective overturning in the North Pacific [*Okazaki et al.*, 2010; *Chikamoto et al.*, 2012; *Rae et al.*, 2014]. In addition to evidence for downwelling in the subarctic Pacific realm during HS1, there is evidence for deglacial upwelling that might have led to enhanced biological productivity during the Bølling-Allerød (B/A) [*Galbraith et al.*, 2007; *Kohfeld and Chase*, 2011]. However, only recently, the high export production during the B/A has rather been related to a transient stratification event [*Lam et al.*, 2013].

A major challenge regarding the reconstruction of changes in upper ocean stratification in the subarctic Pacific realm is the reconstruction of changes in sea surface salinity (SSS), particularly since oxygen isotopic measurements from the most prominent planktic foraminifera *Neogloboquadrina pachyderma* in subarctic Pacific sediments rather reflect subsurface than surface water conditions [*Bauch et al.*, 2002]. Moreover, an evaluation of the actual effect of variations in subarctic Pacific surface water stratification on oceanic-atmospheric CO_2 exchange requires information on the efficiency of the biological pump, which removes CO_2 from the atmosphere by biological productivity in the photic zone and transfers it to the deep ocean interior. Oxygen isotope records from diatoms ($\delta^{18}O_{diat}$), which are photosynthetic algae and thus bound to the photic zone, have been used to trace pulses of freshwater into the Southern Ocean [*Shemesh et al.*, 1994, 2002; *Crespin et al.*, 2014]. Diatom silicon isotope records ($\delta^{30}Si_{diat}$) provide valuable information on changes in the degree of nutrient (silicic acid) utilization in surface waters [*De la Rocha et al.*, 1998; *Reynolds et al.*, 2008; *Maier et al.*, 2013; *Hendry and Brzezinski*, 2014], which is a function of silicic acid (Si)

Table 1. Core Site Summary

Site	Latitude	Longitude	Depth (m)	Core Type
SO202-27-6	54.30	210.40	2929	kasten core
MD02-2489	54.39	211.08	3633	piston core
MD01-2416	51.27	167.73	2317	piston core
SO202-07-6	51.27	167.70	2340	kasten core

supply and use. Thus, $\delta^{30}Si_{diat}$ are useful to assess changes in the efficiency of the biological pump. During biomineralization diatoms preferentially incorporate the lighter isotope (^{28}Si) into their frustules, with a mass-dependent fractionation of about $-1.1 \pm 0.4‰$ [*De la Rocha et al*., 1997; *Milligan et al*., 2004] for a closed system like the subarctic Pacific surface water layer [*Reynolds et al*., 2006], where nutrients (e.g., Si, nitrate, and iron) are brought to the euphotic zone by vertical mixing during autumn/winter [*Harrison et al*., 1999]. The recent study of *Maier et al*. [2013] shows the potential of a combined interpretation of $\delta^{18}O_{diat}$ and $\delta^{30}Si_{diat}$ records for paleoclimate reconstructions in the subarctic NW Pacific, but the records only document conditions since the Bølling and do not reach back to the last glacial.

Here we present the first combined $\delta^{18}O_{diat}$ and $\delta^{30}Si_{diat}$ records from the subarctic northeast (NE) Pacific (Core SO202-27-6, Patton Seamount, Alaskan Gyre; Figure 1a) at millennial-scale resolution over the last glacial-to-interglacial transition to investigate the developments of surface water stratification, Si utilization, and the efficiency of the biological pump in the open subarctic NE Pacific. The isotopic results are compared to deglacial (Bølling-to-Holocene) $\delta^{18}O_{diat}$ and $\delta^{30}Si_{diat}$ records from the NW Pacific (Core MD01-2416, Detroit Seamount, Western Subarctic Gyre) [*Maier et al*., 2013, this study] and are interpreted in combination with other new data from the NE Pacific (Core SO202-27-6: subsurface foraminiferal *N. pachyderma*$_{sin}$ stable isotope ($\delta^{18}O_{Nps}$; $\delta^{13}C_{Nps}$), alkenone-based sea surface temperature (SST), sea ice (IP_{25} concentrations), X-ray fluorescence (XRF), and biogenic opal data; Core MD02-2489: diatom counting data) and from the NW Pacific (Core MD01-2416: diatom counting data; SO202-07-6: sea ice data (IP_{25} concentrations)) (Figure 1a and Table 1). The reconstructed spatiotemporal evolution of the subarctic Pacific upper ocean stratification and Si utilization allows for an updated view on modern paleoceanographic debates concerning the subarctic Pacific realm. We particularly provide new insights in the relative timing of deglacial subarctic Pacific to North Atlantic climate evolution and the role of the subarctic Pacific during the last deglacial atmospheric CO_2 development.

2. Modern Regional Surface Water Oceanography and Water Mass Formation

The surface circulation in the modern subarctic Pacific is dominated by the wind-driven cyclonic motion of the Subarctic Gyre, which contains two prominent cyclonic circulation systems: the Western Subarctic Gyre in the west and the Alaskan Gyre in the east (Figure 1b). The circulation in the coastal area of the NE Pacific is largely isolated from the open ocean circulation, but confined to the Alaskan Coastal Current, which is strongly influenced by freshwater input from the coast [*Allen et al*., 1983; *Stabeno et al*., 2004]. There is a W-E gradient regarding sea surface salinity (SSS), with the NE Pacific surface waters being slightly fresher compared to NW Pacific surface waters (Figure 1b) [*Antonov et al*., 2010]. This W-E difference is primarily related to the riverine influx of freshwater from the Cordilleran mountains into the NE Pacific, which is transported westward by the Alaskan Stream [*Dodimead et al*., 1963]. Even though the permanent halocline limits vertical mixing between the nutrient-rich deeper waters and the more nutrient-depleted surface waters, subarctic Pacific surface waters are generally characterized by incomplete Si and nitrate utilization (Figure 1a) [*Garcia et al*., 2010]. Particularly in the NW Pacific, these nutrients are not completely consumed over the course of the year, resulting in a W-E gradient of increasing nutrient utilization. While the studied NE Pacific cores SO202-27-6 and MD02-2489 are located in the catchment area of the Cordilleran Ice Sheet (CIS), NW Pacific cores MD01-2416 and SO202-07-6 are located in the center of modern-day incomplete nutrient utilization (Figure 1a).

As a consequence of the halocline no deep water is formed in the modern subarctic Pacific realm. Intermediate water formation is restricted to the marginal Sea of Okhotsk, from where well-ventilated Okhotsk Sea Intermediate Water, produced in coastal polynyas by brine rejection during sea ice formation in winter [*Shcherbina et al*., 2003], leaves via the Kurile Straits, mixes with waters from the Western Subarctic Gyre [*Yasuda*, 1997; *You*, 2003] and further south with Kuroshio waters, thereby forming North Pacific Intermediate Water (NPIW) [*Shimizu et al*., 2004]. Even though NPIW is largely confined to the

subtropical gyre, it also influences the subarctic Pacific [*Reynolds et al*., 2006; *Sarmiento et al*., 2004]. Compared to intermediate waters entering the subarctic Pacific from the south, NPIW is characterized by a relatively high Si content [*Sarmiento et al*., 2004].

3. Material and Methods

3.1. Core Material

We sampled the top 91 cm of Core SO202-27-6 from the Alaskan Gyre (Patton Seamount, NE Pacific) (Figure 1a), which was recovered with a kasten corer (30 × 30 cm dimension) during the Innovative NOrth Pacific EXperiment (INOPEX) cruise in summer 2009 [*Gersonde and SO202-INOPEX Participants*, 2010]. A box from this kasten core (15 × 7.5 × 99 cm) was sampled every 4–5 cm for $\delta^{18}O_{diat}$ and $\delta^{30}Si_{diat}$ analysis (2 cm thick slices; 225 cc), every 4 cm for $\delta^{18}O_{Nps}$ and $\delta^{13}C_{Nps}$ analyses (1 cm thick slices; 112 cc), and for reconstruction of alkenone-based SST and sea ice (IP_{25} concentration) (1 cm thick slices; 15 cc). Furthermore, we sampled the core every 1–4 cm for the determination of the biogenic opal concentration (1 cm thick slices; 7.5 cc). (For exact sample depths see Tables S2–S5 in the supporting information.) In addition, we increased the resolution of the previously published $\delta^{18}O_{diat}$ and $\delta^{30}Si_{diat}$ record from NW Pacific Core MD01-2416 (Figure 1a) [*Maier et al*., 2013] by the intercalation of six new $\delta^{18}O_{diat}$ and $\delta^{30}Si_{diat}$ measurements over the deglacial to Holocene period (4 cm thick slices taken; only half of the core (12 cm diameter) was sampled). Additionally, the upper 80 cm of NW Pacific Core SO202-07-6 (Figure 1a) were sampled every 5–10 cm for the determination of IP_{25} concentrations (1 cm thick slices; 20 cc). We furthermore sampled the upper 200 cm of Core MD01-2416 and the upper 390 cm of Core MD02-2489 every 5–10 cm for the determination of diatom relative abundances (5 cc).

3.2. Preparation and Documentation of Diatom Fraction for Isotopic Analyses

Sixteen bulk samples from kasten Core SO202-27-6, and six bulk samples from piston Core MD01-2416, were prepared for diatom isotope analyses using a combination of physical and chemical treatments [*Maier et al*., 2013]. Briefly, after the bulk samples were liberated from carbonates and organic matter, samples were further prepared using various sieving steps, sonication, and treatments with heavy liquids. After a first heavy liquid separation, where most of the lithic fragments were removed, we chose the 100–125 μm fraction for Core SO202-27-6 to be further purified. To estimate the composition of the diatom assemblages in this fraction, we prepared microscopic slides prior to the sonication procedure, since sonication led to the shattering of diatom valves, which precluded the determination of the diatom assemblages in the final purified samples. On average ~200 biogenic opal components (diatoms, radiolarians, and sponge spicules) were counted using a Zeiss Axioskop I at 400X magnification, following the counting approach described in *Maier et al*. [2013]. Diatoms were identified following the taxonomy of *Sancetta* [1982, 1987]. Following continuative sonication to separate the majority of radiolarians and sponge spicules from the diatom material (Figure S1), the actual contribution of radiolarians and sponge spicules to the final purified diatom samples was then estimated under a Philips XL 30 Environmental scanning electron microscope by counting on average ~340 silica particle equivalents at 350X magnification. The estimation of the radiolarian/sponge spicule content in the final purified diatom samples is particularly important for the $\delta^{30}Si_{diat}$ record, since diatoms generally harbor positive silicon isotope values [e.g., *De la Rocha et al*., 1998; *Brzezinski et al*., 2002; *Maier et al*., 2013], while $\delta^{30}Si$ values of radiolarians and siliceous sponge spicules may be as low as about −3.1‰ (A. Abelmann, unpublished data) and −5.7‰ [*Hendry and Robinson*, 2012], respectively. Concerning Core MD01-2416, we purified the >63 μm fraction to obtain results comparable to the samples presented by *Maier et al*. [2013].

As contamination with nonbiogenic silicates (e.g., rock fragments and clay minerals) may influence especially the oxygen isotope value of biogenic silica [*Brewer et al*., 2008], all purified diatom samples were checked for such contamination using energy-dispersive X-ray spectrometry (EDS) [*Chapligin et al*., 2012; *Maier et al*., 2013]. At two depths of Core SO202-27-6 (10 cm and 22 cm) additional inductively coupled plasma optical emission spectrometry measurements according to *Chapligin et al*. [2012] were performed to assure on the validity of the EDS measurements. We used Al_2O_3 as a tracer for contamination of nonbiogenic silicates [*Brewer et al*., 2008] following the quantification approach described by *Maier et al*. [2013]. To decipher the influence of nonbiogenic silicates on the measured $\delta^{18}O_{diat}$ and $\delta^{30}Si_{diat}$ signals, we used mass balance

corrections based on *Swann and Leng* [2009], thereby removing the potential isotopic effects of the nonbiogenic silicates according to the following equations:

$$\delta^{18}O_{cont-corr} = \left(\delta^{18}O_{diat} - \left(\%cont\ x\delta^{18}O_{cont}\right)\right)/\%purity \quad (1)$$

$$\delta^{30}Si_{cont-corr} = \left(\delta^{30}Si_{diat} - \left(\%cont\ x\delta^{30}Si_{cont}\right)\right)/\%purity \quad (2)$$

where $\delta^{18}O_{cont\text{-}corr}$ and $\delta^{30}Si_{cont\text{-}corr}$ are the $\delta^{18}O_{diat}$ and $\delta^{30}Si_{diat}$ values corrected for contamination with nonbiogenic silicates, $\delta^{18}O_{diat}$ and $\delta^{30}Si_{diat}$ are the measured isotopic values, %cont is the EDS-determined nonbiogenic silicate contamination, and $\delta^{18}O_{cont}$ and $\delta^{30}Si_{cont}$ are the isotopic values for the contamination. The $\delta^{30}Si$ of nonbiogenic silicates generally ranges between about −2.5 and +1.8‰ [*Douthitt*, 1982; *Ding et al*., 1996; *Ziegler et al*., 2005], while their $\delta^{18}O_{cont}$ signal usually ranges from +2 to +30‰ [*Taylor*, 1968; *Sheppard and Gilg*, 1996]. To cover the possible range of the influence from such a contamination, we applied two different $\delta^{18}O_{cont}$ values (+2‰ and +30.00‰) and $\delta^{30}Si_{cont}$ values (−2.50‰ and +1.80‰).

3.3. Stable Isotope Measurements

To monitor surface water conditions, 22 purified diatom samples (16 samples from Core SO202-27-6 and six samples from Core MD01-2416) were measured at the Alfred Wegener Institute Helmholtz Centre for Polar and Marine Research (AWI) (Potsdam and Bremerhaven), using combined silica $\delta^{18}O$ and $\delta^{30}Si$ analyses according to *Maier et al*. [2013] and *Chapligin et al*. [2010]. Values are reported in the common δ notation versus Vienna Standard Mean Ocean Water (V-SMOW) for oxygen isotopes and versus National Bureau of Standards-28 (NBS-28) for silicon isotopes, using the laboratory diatom standards PS1772-8_{bsis} (marine) and BFC (lacustrine) calibrated against the International Atomic Energy Agency reference quartz standard NBS-28. Repeated analyses of PS1772-8_{bsis} and BFC over the period of about 8 weeks when SO202-27-6 diatom samples were measured show an analytical precision better than 0.24‰ for $\delta^{18}O_{diat}$ (1σ; $n = 67$ for PS1772-8_{bsis}; $n = 10$ for BFC) and better than 0.12‰ for $\delta^{30}Si_{diat}$ measurements (1σ; $n = 62$ for PS1772-8_{bsis}; $n = 7$ for BFC). This is in line with published long-term analytical reproducibility for silica $\delta^{18}O$ and $\delta^{30}Si$ from this instrumentation [*Chapligin et al*., 2011; *Maier et al*., 2013]. Diatom samples were measured at least twice when enough purified material was available.

Information on the subsurface water development was achieved by analyzing the $\delta^{18}O$ values of the planktic foraminifer *N. pachyderma*$_{sin}$, which are believed to calcify at the bottom of the thermocline [*Bauch et al*., 2002]. *Neogloboquadrina pachyderma*$_{sin}$ were picked from the 125–250 μm (19 samples), the 315–400 μm (two samples), and the >400 μm (one sample) fraction. Isotope measurements were performed at the AWI (Bremerhaven) using a MAT 251 mass spectrometer directly coupled to an automated carbonate preparation device (Kiel I) and calibrated via National Institute of Standards and Technology-19 international standard (NIST-19) to the Pee Dee belemnite (PDB) scale. All values are given in δ notation versus Vienna PDB. The precision of the measurements, based on repeated analyses of an internal laboratory standard (Solnhofen limestone) over a 1 year period, was better than 0.08‰ (1σ).

3.4. Alkenone-Based SST and Sea Ice Proxy IP_{25}

Alkenone-based SST and IP_{25} concentrations were determined using gas chromatography (GC) and GC-mass spectrometry according to the procedures described in *Méheust et al*. [2013]. SSTs were determined using the *Sikes et al*. [1997] calibration, which has been shown to provide reasonable summer SST estimates for the (sub)arctic Pacific [*Méheust et al*., 2013]. The standard error of the calibration is reported as 1.5°C. The total analytical error calculated by replicate analyses of an external alkenone standard (extracted from Ehux cultures with known growth temperature) is less than 0.4°C. IP_{25} is a highly branched isoprenoid alkene with 25 carbon atoms, which is produced by certain sea ice diatoms during the spring bloom period [*Belt et al*., 2007; *Brown et al*., 2014]. Surface sediment studies have demonstrated the biomarker IP_{25} to be a valuable proxy for reconstructing the presence of sea ice in the (sub)arctic Pacific [*Méheust et al*., 2013; *Stoynova et al*., 2013; *Brown et al*., 2014]. Based on these studies and the concept of *Müller et al*. [2011], we used IP_{25} as a qualitative indicator for sea ice.

3.5. Estimation of Local Surface Seawater $\delta^{18}O$ ($\delta^{18}O_{sw}$)

We calculated the local surface $\delta^{18}O_{sw}$ to approximate past changes in sea surface salinity (SSS) in the NE Pacific by correcting the $\delta^{18}O_{diat}$ record of Core SO202-27-6 for temperature and global ice volume. First,

$\delta^{18}O_{diat}$ was corrected for temperature using alkenone-based SSTs from the same core and following the approach of *Juillet-Leclerc and Labeyrie* [1987]:

$$\text{local surface } \delta^{18}0_{sw} = \delta^{18}0_{diat} - 34 - \sqrt{122 - 5SST} \quad (3)$$

where local surface $\delta^{18}O_{sw}$ is the local surface seawater $\delta^{18}O$, $\delta^{18}O_{diat}$ is the measured diatom $\delta^{18}O$, and SST is the temperature calculated from the alkenone-based SST record from the same core. Since samples for alkenone-based SST were not from the exact same depths as the diatom isotope samples, the corresponding temperatures were determined through linear interpolation. The temperature-corrected record was then additionally corrected for global ice volume, using the data of *Waelbroeck et al*. [2002], which were also linearly interpolated to get data for the same points of time. Considering the poor knowledge of the relationship between salinity and $\delta^{18}O_{sw}$ for the studied site, we used the approximated local surface $\delta^{18}O_{sw}$ as first-order indicator for changes in SSS. The errors in local surface $\delta^{18}O_{sw}$ were estimated by propagating the error introduced by the $\delta^{18}O_{diat}$ and alkenone measurements, the alkenone:temperature calibration, and the removal of global ice volume and are about 0.44‰ (see Figure S2).

3.6. XRF Core Logging

The relative elemental composition (counts per second; cps) of Core SO202-27-6 was measured at 1 cm resolution using an Avaatech X-ray fluorescence (XRF) core scanner located at the AWI (Bremerhaven). Altogether three measurements were performed at 1 mA with varying tube voltages (10 kV, 30 kV, and 50 kV) to allow for the mapping of a large quantity of elements. Counting time was set to 30 s. The relatively light elements Si, Fe, and Ca presented here were obtained from the scan at 10 kV. We used the Fe and Ca XRF records to help create an age model (see section 4) and the Si/Fe ratio as supporting information on relative changes in the content of biogenic opal within the sediment.

3.7. Biogenic Opal

We determined the concentration of biogenic opal within 33 bulk samples of Core SO202-27-6 at the AWI (Bremerhaven), following the automated leaching method of *Müller and Schneider* [1993] and using an amount of approximately 20 mg. Biogenic opal (weight percent) values were calculated from the biogenic silica concentration adding 10% H_2O bound in the skeleton and correcting for the concentrations of salt in the input sample after *Kuhn* [2013]. Weight percent of biogenic opal from 10 samples, of which we had information on dry bulk density, were converted into mass accumulation rates (MARs) of opal to compensate for the effects of percentage dilution of biogenic silica by other sediment particles. As supporting information on relative changes in the concentration of biogenic opal we used the Si/Fe ratio from XRF core logging (see section 3.4). We use the changes in biogenic opal concentration, opal mass accumulation rates (MARs), and Si/Fe as indicators for changes in opal deposition.

3.8. Diatom Counting

Quantitative diatom slides from cores MD01-2416 (31 slides) and MD02-2489 (44 slides) were prepared according to the standard procedure established by *Gersonde and Zielinski* [2000]. Diatom counting was done following the description of *Schrader and Gersonde* [1978]. An average of 400 diatom valves was counted for each sample using a Zeiss Axioskop microscope at 1000X magnification. Diatoms were identified to species or species group level according to *Ren et al*. [2014, and references therein]. The observed *Chaetoceros* specimens belong to the subgenus *Hyalochaetae*, whose resting spores were not possible to be identified to species level due to the absence of setae. Therefore, we grouped resting spores of different *Chaetoceros* species into *Chaetoceros* resting spores (r. sp.).

3.9. Radiocarbon

Six samples of pristine specimens of the planktic foraminifer *N. pachyderma*$_{sin}$ were picked from the 125–250 μm fraction of Core SO202-27-6 and analyzed for radiocarbon by accelerator mass spectrometry (AMS) at the National Ocean Science AMS facility at Woods Hole Oceanographic Institution (Table 2). Foraminifera were not cleaned before radiocarbon analysis.

Table 2. Planktic (*N. pachyderma*$_{sin}$) Radiocarbon Ages and Calibrated Ages of Core SO202-27-6[a]

Sample ID	Depth (cm)	^{14}C Ages (ka)	^{14}C Age Error (a)	Reservoir Age (a)	Calibrated Ages (ka B.P.)	Derivation of Cal Age	Calib 7.1 Calibrated Ages (ka B.P.) Median (ka B.P.)	2σ Min (ka B.P.)	2σ Max (ka B.P.)	Relative Area Under Probability Distribution
OS-85661	0.5	6.090	30	440 ± 285	**6.493**	Calib 7.1	6.493	5.878	7.156	1
OS-85752	12.5	9.880	30	440 ± 285	**10.781**	Calib 7.1	10.781	10.077	11.681	1
-	26.5	-	-	440 ± 285	**14.050**	Plateau I top	-	-	-	-
OS-87903	28.5	13.050	55	440 ± 285	14.239	Plateau I	-	-	-	-
-	37.5	-	-	440 ± 285	**14.920**	Plateau I base	-	-	-	-
-	39.5	-	-	550 ± 305	**15.250**	Plateau IIa top	-	-	-	-
OS-85753	44.5	13.900	30	550 ± 305	15.721	Plateau IIa	-	-	-	-
-	48.0	-	-	550 ± 305/120	**16.050**	P IIa base/P IIb top	-	-	-	-
-	51.0	-	-	550 ± 120	**16.400**	P IIb base	-	-	-	-
OS-87888	72.5	18.750	70	1110 ± 334	**21.321**	Calib 7.1	21.321	20.485	22.214	1
OS-87894	88.5	21.400	120	1110 ± 334	**24.435**	Calib 7.1	24.435	23.576	25.336	1

[a]Reservoir ages were assigned from nearby Core MD02-2489 [*Sarntheim et al.*, 2015]. In bold: age control points.

4. Chronologies for Cores MD01-2416, MD02-2489, and SO202-27-6

The age models of cores MD01-2416 and MD02-2489 are primarily based on ^{14}C plateau tuning [see *Sarntheim et al.*, 2015], where marine ^{14}C plateaus, detected within the high-resolution ^{14}C records of cores MD01-2416 and MD02-2489 [*Gebhardt et al.*, 2008; *Sarntheim et al.*, 2015], were correlated to atmospheric ^{14}C plateaus, identified within the well-calibrated, high-resolution Lake Suigetsu record of atmospheric ^{14}C [*Bronk Ramsey et al.*, 2012]. Outside of the ^{14}C plateaus we calculated calendar years (1000 cal years B.P. = 1 ka B.P.) from the raw ^{14}C ages [*Sarnthein et al.*, 2004, 2007; *Gebhardt et al.*, 2008] using the CALIB 7.1 software and the Marine13 calibration data set [*Stuiver and Reimer*, 1993; *Reimer et al.*, 2013] (Table S1). For the calibration we applied the reservoir ages determined by *Sarntheim et al.* [2015] for the respective ^{14}C plateaus (Figure 2 and Table S1).

To create the age model for Core SO202-27-6, we used its proximity to Core MD02-2489. By correlating XRF and biogenic opal data, we first assigned a suite of three ^{14}C plateaus (plateaus I, IIa, and IIb) [*Sarntheim et al.*, 2015] to Core SO202-27-6 (Figure 2). This assignment provides five age control points (the calibrated ages of the ^{14}C plateau boundaries). Outside of the plateaus we calibrated the raw ^{14}C ages of Core SO202-27-6 with the CALIB 7.1 software as described above, using different reservoir ages (Table 2). We applied a reservoir age of 440 ± 285 years for the two ^{14}C values above Plateau I and of 1100 ± 334 years for the two ^{14}C values below Plateau IIb, which correspond to the reservoir ages determined by *Sarntheim et al.* [2015] for the time of the ^{14}C plateau closest to the ^{14}C age. In between the nine determined age control points we used linear interpolation.

Considering the poor knowledge of paleoreservoir ages in the subarctic Pacific realm, we tested our age model for Core SO202-27-6 by plotting the diatom isotopic data additionally on three age models, which were solely based on calibrated planktic ^{14}C ages and linear interpolation in between, using different paleoreservoir ages previously applied for the subarctic Pacific realm (Figure S3). This comparison shows that even though the ages of single isotopic data points can vary by a maximum of 500–850 years depending on the age model, the main changes of the isotopic signals as discussed below occur within the same time intervals independent from the choice of the age model, highlighting the robustness of our findings.

5. Results

5.1. Reliability and Significance of the $\delta^{18}O_{diat}$ and $\delta^{30}Si_{diat}$ Records

The reliability of $\delta^{18}O_{diat}$ and $\delta^{30}Si_{diat}$ records to reflect changes in surface water parameters (SSS, SST, and Si utilization) strongly depends on the quality of the isotopic data and the knowledge on environmental and biological factors affecting the isotopic signal. It is thus crucial to assess the impact of factors potentially biasing the isotopic signal such as contamination by nondiatom silicates and species-related isotope effects (vital and environmental/seasonal effects). Equally, the primary environmental factors, which control the

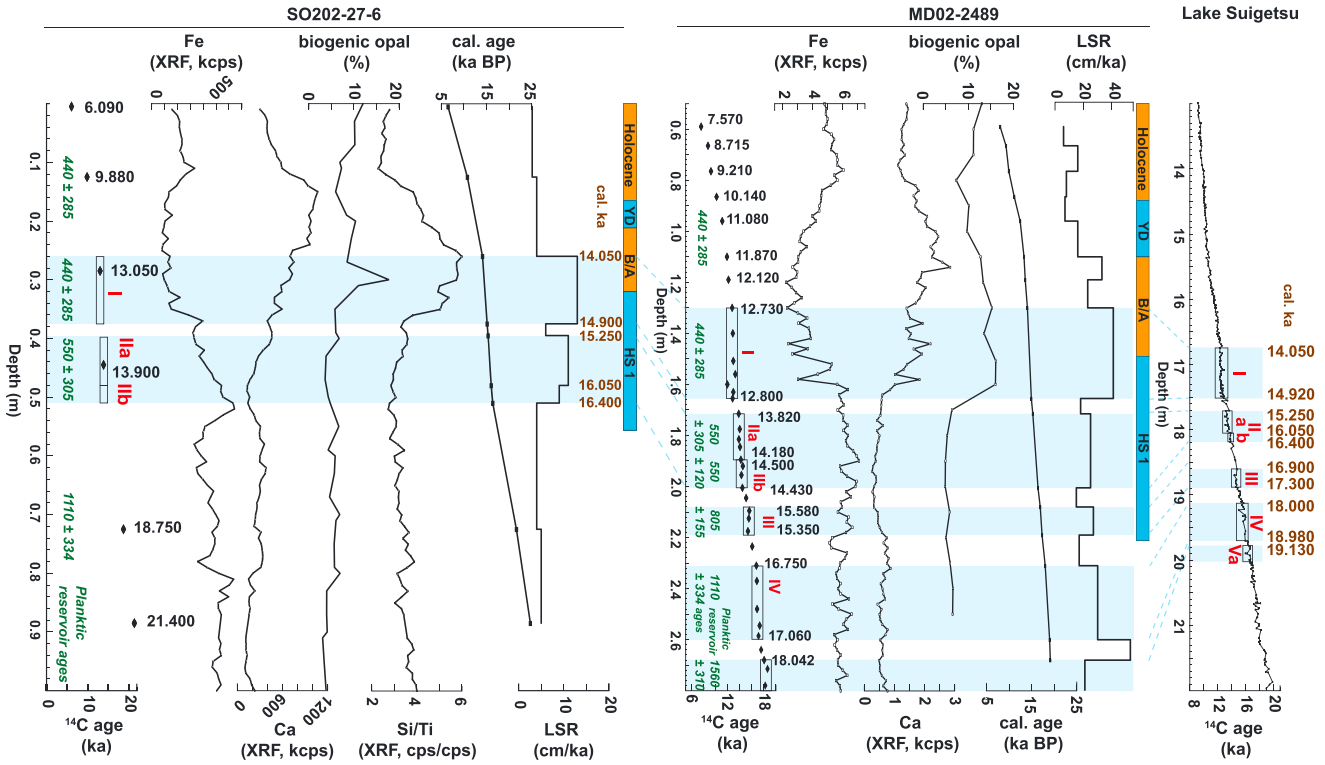

Figure 2. Age models of Core SO202-27-6 and MD02-2489 including linear sedimentation rates (LSR). The Lake Suigetsu record of atmospheric ^{14}C is taken from *Bronk Ramsey et al.* [2012] and ^{14}C plateau boundaries displayed after *Sarntheim et al.*, 2015. MD02-2489: biogenic opal and XRF data taken from *Gebhardt et al.* [2008], planktic ^{14}C record taken from *Gebhardt et al.* [2008] and *Sarntheim et al.* [2015], and ^{14}C plateau boundaries and planktic reservoir ages from *Sarntheim et al.* [2015].

generation of the isotopic signals, should be determined to allow for appropriate paleoenvironmental interpretation, e.g., concerning physical water properties (SST, SSS, and stratification) and Si utilization (Si supply versus use). This issue can best be achieved by the combination of the diatom isotopic signals and considering environmental information obtained with other proxies (e.g., for SST, biogenic deposition).

Contamination with nonbiogenic silicates (e.g., minerals and rock fragments) is generally below 4.0% for all measured diatom samples from both sediment cores (SO202-27-6 and MD01-2416) (Table S2), with two exceptions regarding Core SO202-27-6: the core top sample (4.2%) and the lowermost sample of the studied core section (6.0%). Since the mass balance corrections for Core SO202-27-6 based on these results show only a shift of the isotopic signals, which does not change the overall deglacial to Holocene patterns (Figure S4), the large amplitudes occurring in the isotopic records are not attributed to contamination with nonbiogenic silicates. *Maier et al.* [2013] demonstrated that the effects of nondiatom biogenic silicates, in particular radiolarians and sponge spicules, on the isotopic signals are negligible for the MD01-2416 diatom samples. We regard that this is also true for the isotopic signals from Core SO202-27-6, considering the low content of radiolarians (~5%) and sponge spicules (≤1%) in the purified diatom samples (Table S3).

Maier et al. [2013] showed that the diatom species composition of the >63 μm fraction of Core MD01-2416 solely (98.5–100%) consists of the species belonging to the genus *Coscinodiscus*. Qualitative checking of the diatom composition of all new complementary MD01-2416 diatom samples under the light microscope and the scanning electron microscope confirm the absolute dominance of *Coscinodiscus* species. The SO202-27-6 diatom samples were also dominated (93.7–100%) by *Coscinodiscus* species, with a strong dominance of *C. marginatus* (83–98%) over *C. oculus-iridis* (2–11%) (Table S3). There is no significant correlation between the diatom species composition and $\delta^{18}O_{diat}$ or $\delta^{30}Si_{diat}$ values ($R^2 \leq 0.19$; $P \geq 0.10$), indicating no discernable species-related isotope effects biasing the isotopic records. This can be partly explained by a similar ecology of both *Coscinodiscus* species, as indicated by sediment trap studies from the subarctic Pacific showing major fluxes of both *C. marginatus* and *C. oculus-iridis* during the same season (autumn/early winter) [*Takahashi*, 1986; *Takahashi et al.*, 1990; *Onodera et al.*, 2005]. Moreover, culture

studies on different diatom species from different suborders (including *Coscinodiscus* sp.) [*Brandriss et al*., 1998; *Schmidt et al*., 2001] show no unequivocal evidence of vital effects on $\delta^{18}O_{diat}$, suggesting vital effects for $\delta^{18}O_{diat}$ unlikely to occur between both *Coscinodiscus* species. Concerning $\delta^{30}Si_{diat}$, the recent culture study of *Sutton et al*. [2013] indicates limited evidence of species-specific fractionation, but so far, no study has investigated the Si fractionation of *Coscinodiscus* species. However, the genus *Coscinodiscus* belongs to the same suborder as the genus *Thalassiosira*, for which culture studies showed variations in the fractionation factor ε between −0.92‰ and −1.50‰ [*De la Rocha et al*., 1997; *Milligan et al*., 2004; *Sutton et al*., 2013; *Sun et al*., 2014]. Assuming a similar range in ε for the genus *Coscinodiscus*, Si utilization calculations from the $\delta^{30}Si_{diat}$ record show that even when a difference in ε of 0.58‰ between both *Coscinodiscus* species is applied (−0.92‰ for *C. marginatus* and −1.50‰ for *C. oculus-iridis*, and vice versa), the resulting Si utilization still mirrors the pattern of the $\delta^{30}Si_{diat}$ record (Figure S5). Thus, considering the purity of the measured diatom samples and the absence of discernable species-related isotope effects, the isotopic signals are considered to be reliable proxies for temporal changes in surface water hydrography and relative changes in Si utilization.

In NE Pacific Core SO202-27-6 the $\delta^{18}O_{diat}$ record varies by about 4.0‰ between high $\delta^{18}O_{diat}$ values during the B/A and the YD (about +43.6‰) and low $\delta^{18}O_{diat}$ values during HS1 (+41.1‰) and the early Holocene (about +40.0‰) (Figure 3a and Table S4). The $\delta^{18}O_{diat}$ record shows the same deglacial pattern as the reconstructed local surface $\delta^{18}O_{sw}$ record (Figure 3a). This suggests that $\delta^{18}O_{diat}$ is strongly controlled by SSS variability, while the effect of SST (Figure 3e) and global ice volume is minor (Figure S2). Hence, the $\delta^{18}O_{diat}$ signal can be interpreted to mirror changes in SSS, such as glacial and deglacial meltwater events in the catchment area of the CIS (Figure 1a). The $\delta^{18}O_{diat}$ record from NW Pacific Core MD01-2416 exhibits similar absolute $\delta^{18}O_{diat}$ values around +43.9‰ during the B/A and YD (Figure 3j and Table S4), but the early Holocene decrease in $\delta^{18}O_{diat}$ in the NE Pacific is nearly 3 times larger than the decrease in the NW Pacific (Figures 3a and 3j and Table S4). In contrast to the NE Pacific, where the local surface $\delta^{18}O_{sw}$ record indicates an early Holocene decrease in SSS equal to a decrease in $\delta^{18}O_{sw}$ of about 2.0‰, the early Holocene decrease in $\delta^{18}O_{diat}$ of about 1.4‰ can largely be explained by changes in global ice volume and SST increase of about 4°C [*Max et al*., 2012], assuming a relationship between $\delta^{18}O_{diat}$ and water temperature of about −0.2‰/°C [*Dodd and Sharp*, 2010].

The $\delta^{30}Si_{diat}$ values of NE Pacific Core SO202-27-6 vary by about 0.8‰, with low values during early HS1 (about +1.2‰), high values during mid-HS1 and the early Holocene (about +2.0‰), and values in between during the last glacial and the B/A and YD (Figure 3b). The correlation between $\delta^{30}Si_{diat}$ and $\delta^{18}O_{diat}$ values ($R^2 = 0.46$; $P < 0.01$) indicates a relatively close relationship between relative changes in Si utilization (Si supply versus use) and SSS. Since high $\delta^{30}Si_{diat}$ values are generally not coupled to high opal deposition and vice versa (Figures 3b and 3c), the observed pattern in $\delta^{30}Si_{diat}$ seems to be dominantly modulated by changes in the supply of Si to the euphotic zone rather than net Si use. Changes in the supply of bioavailable iron to surface waters, which could affect Si utilization by influencing diatom productivity, diatom physiology [*Takeda*, 1998], and/or phytoplankton community [*Marchetti et al*., 2006; *Tsuda et al*., 2007], seem to be only of subordinate importance. In NW Pacific Core MD01-2416, $\delta^{30}Si_{diat}$ and $\delta^{18}O_{diat}$ values are not correlated ($R^2 = 0.01$; $P = 0.72$) (Figures 3j and 3k), suggesting a more complex deglacial relationship between both proxies. However, while similar, relatively low, $\delta^{30}Si_{diat}$ values during the B/A and the early Holocene (about +1.3‰) indicate a similar degree of Si utilization during both times, the increased biogenic opal concentrations during the B/A (Figure 3l) [*Gebhardt et al*., 2008] point toward a relatively increased Si supply during the B/A.

5.2. Sequence of Paleoceanographic Events in Subarctic Pacific Surface Waters Since the Last Glacial

Diatom isotopic records from Core SO202-27-6 provide paleoceanographic information about the evolution of subarctic NE Pacific surface waters from the last glacial to the Holocene, and the diatom isotopic records from NW Pacific Core MD01-2416 allow for an additional spatial reconstruction of surface water evolution since the Bølling (Figure 3). The deglacial pattern of the NE Pacific subsurface $\delta^{18}O_{Nps}$ does not mirror the surface $\delta^{18}O_{diat}$ pattern (Figures 3a and 3f), but the glacial-interglacial change in $\delta^{18}O_{Nps}$ of about 1.3‰ largely corresponds to the mean global glacial-interglacial changes in seawater $\delta^{18}O_{sw}$ [*Waelbroeck et al*., 2002] and an increase in subsurface temperature of about 2–3°C [*Gebhardt et al*., 2008] (assuming a relationship between temperature and $\delta^{18}O_{Nps}$ of −0.28°C/‰ [*Mulitza et al*., 2003]). This indicates largely decoupled paleoclimatic evolutions of NE Pacific surface and subsurface waters.

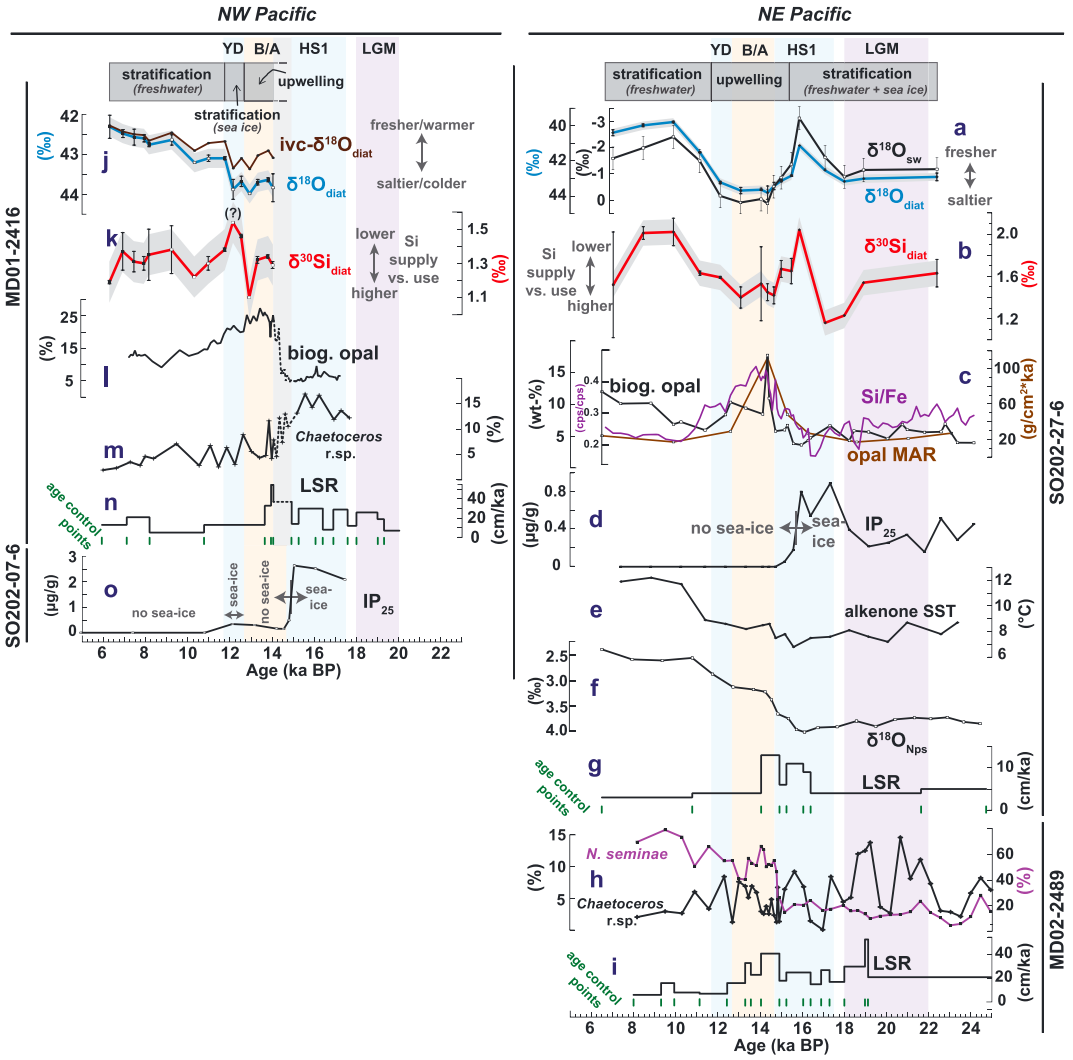

Figure 3. Proxy data of cores from the (a–l) NE Pacific (SO202-27-6 and MD02-2489) and (m–o) NW Pacific (MD01-2416 and SO202-07-6) and interpretation of changes in surface water hydrography. SO202-27-6 (Figures 3a–3g): Figure 3a shows $\delta^{18}O_{diat}$ and local surface $\delta^{18}O_{sw}$ ($\delta^{18}O_{diat}$: error bars indicate errors of replicate analyses (1σ), and grey envelope indicates long-term reproducibility of standards (1σ); local surface $\delta^{18}O_{sw}$: error bars indicate errors estimated by propagating the errors introduced by the $\delta^{18}O_{diat}$ measurements, the alkenone measurements, the alkenone:temperature calibration, and the removal of global ice volume (see section 3.5)). Figure 3b shows $\delta^{30}Si_{diat}$ (error bars indicate errors (1σ) of replicate analyses, and grey envelope indicates long-term reproducibility of standards (1σ)). Figure 3c shows biogenic opal, opal MAR, and Si/Fe ratio. Figure 3d shows IP_{25} concentration. Figure 3e shows alkenone-based SST. Figure 3f shows $\delta^{18}O_{Nps}$. Figure 3g shows LSR including age control points. MD02-2489 (Figures 3h and 3i) (on timescale presented in this paper): Figure 3h shows *Chaetoceros* r. sp. and *N. seminae* relative abundances, and Figure 3i shows LSR including age control points. MD01-2416 (Figures 3j–3o) (on timescale presented in this paper): Figure 3j shows $\delta^{18}O_{diat}$ ([*Maier et al.*, 2013]: black squares; this study: open squares) (error bars and grey envelope as described in Figure 3a) and ice volume-corrected $\delta^{18}O_{diat}$ [after *Waelbroeck et al.*, 2002]. Figure 3k shows $\delta^{30}Si_{diat}$ ([*Maier et al.*, 2013]: black squares; this study: open squares) (error bars and grey envelope as described in Figure 3b). The isotopic value marked with a question mark is the average value based on two replicate measurements (+1.17‰ and +1.90‰). The great difference between both measurements suggests that one of these measurements was biased. Figure 3l shows biogenic opal [*Gebhardt et al.*, 2008]. Figure 3m shows *Chaetoceros* r. sp. relative abundances. Figure 3n shows LSR including age control points. The grey vertical box marks the ^{14}C plateau that includes the HS1-B/A boundary. This boundary cannot be determined more precisely (see section 4 and section 6.2.)) for Core MD01-2416. Figure 3o shows IP_{25} concentration data from Core SO202-07-6. The age model of Core SO202-07-6 is based on the correlation of dust fluxes to North Greenland Ice Core Project (NGRIP) dust fluxes, in combination with *N. pachyderma* radiocarbon ages [*Serno et al.*, 2015].

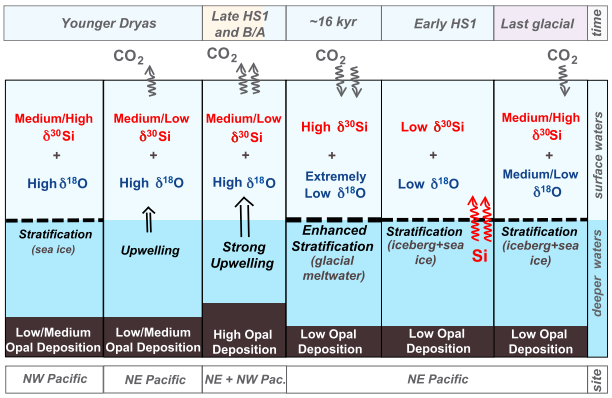

Figure 4. Summarizing scheme of deglacial changes in subarctic Pacific $\delta^{30}Si_{diat}$, $\delta^{18}O_{diat}$, and opal deposition as well as inferred changes in surface water stratification, upwelling, and CO_2 degassing. NW Pacific opal deposition after *Gebhardt et al.* [2008].

From the last glacial to mid-HS1 diatom isotopic results generally indicate freshwater-related stratified surface waters in the NE Pacific, likely due to glacial meltwater from the CIS, which limit the Si supply to surface waters (Figure 4). The presence of sea ice, as indicated by the presence of IP_{25} (Figure 3d), points to an even further enhanced stratification due to melting sea ice. The exceptional situation of an increased Si supply during early HS1, when surface waters were still stratified, can be explained by an increased Si content in subsurface and/or intermediate waters, which constitute the major source of nutrients for phytoplankton in the open subarctic Pacific (Figures 3b and 4). Recent studies showed an increased formation rate of NPIW during HS1 [*Jaccard and Galbraith*, 2013; *Max et al.*, 2014]. Since NPIW influences the entire modern North Pacific [*Reynolds et al.*, 2006; *Sarmiento et al.*, 2004] and is characterized by a relatively high Si content [*Sarmiento et al.*, 2004], we suggest that the increased intensity of NPIW formation during HS1 has led to an increased lateral supply of Si to NE Pacific subsurface/intermediate waters, which was then transported to surface waters via upwelling or diapycnal mixing. During early-to-mid HS1 our $\delta^{18}O_{diat}$/local surface $\delta^{18}O_{sw}$ data indicate even fresher surface waters compared to the last glacial. Such a freshwater anomaly, however, is not mirrored by subsurface $\delta^{18}O_{Nps}$ (Figure 3f), indicating that it was restricted to surface waters.

Relatively saline surface waters in combination with an excess Si supply during the B/A and YD point to a breakdown in NE Pacific surface water stratification, starting in late HS1 B.P. (Figure 4), in coincidence with a switch to sea ice free-conditions, an increase in alkenone-based SST of about 1.5°C and an increase in subsurface $\delta^{18}O_{Nps}$ (Figures 3d–3f). The excess Si supply also to NW Pacific surface waters during the B/A [see also *Maier et al.*, 2013], together with similar absolute $\delta^{18}O_{diat}$ values in the NE and NW Pacific (about +43.9‰) (Figures 3a and 3j), points to a uniform pattern of subarctic Pacific upwelling during the B/A. In situ iron fertilization experiments in the iron-limited subarctic Pacific showed a high growth rate of *Chaetoceros* species upon iron addition [*Takeda and Tsuda*, 2005; *Takeda*, 2011]. Thus, the low relative abundances of *Chaetoceros* r. sp. in bulk sediments from the NE and NW Pacific during the B/A (Figures 3h and 3m) indicate that incomplete Si utilization is likely linked to iron limitation, even though the flux of airborne iron via dust in the subarctic Pacific is still higher during the B/A compared to the early Holocene [*Lam et al.*, 2013; *Serno et al.*, 2015].

While diatom isotopic data indicate that there was still upwelling in the NE Pacific during the YD, we suggest that the combination of unchanged high $\delta^{18}O_{diat}$ but slightly increased $\delta^{30}Si_{diat}$ (by about 0.2‰) in the NW Pacific is indicative of stratified surface waters, related to melting sea ice (Figure 4). Such a scenario, based on the fact that sea ice formation/melting has no significant effect on $\delta^{18}O_{sw}$ [*Craig and Gordon*, 1965; *Meredith et al.*, 2008], was previously suggested by *Maier et al.* [2013]. We increase robustness to this hypothesis by adding new $\delta^{18}O_{diat}$ and $\delta^{30}Si_{diat}$ data covering the YD as well as by providing evidence for the presence of sea ice at the study site during the YD (indicated by the presence of IP_{25} in YD sediments of Core SO202-07-6) (Figures 1a and 3o). Note that the standard deviation of the highest $\delta^{30}Si_{diat}$ value during the YD, composed of two isotopic measurements, is exceptionally high (0.52‰, 1σ). Unfortunately, we could not perform a third measurement since there was not enough purified diatom material available. Nevertheless, even without this data point, the record shows an increase in Si utilization following the B/A.

Following the YD, the larger decrease in $\delta^{18}O_{diat}$ in the NE Pacific compared to the NW Pacific indicates a relatively lower SSS in the early Holocene NE Pacific (Figures 3a and 3j). A W-E difference can also be observed concerning the evolution of early Holocene Si utilization (Figures 3b and 3k). However, both observations might

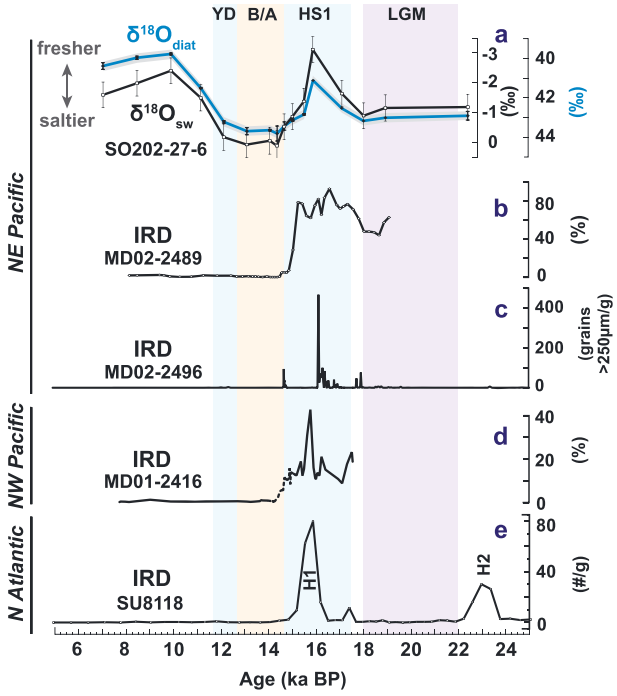

Figure 5. (a) $\delta^{18}O_{diat}$ and local surface $\delta^{18}O_{sw}$ from NE Pacific Core SO202-27-6 (error bars and grey envelope as delineated in Figure 3). (b–e) IRD data from NE Pacific Core MD02-2489 (on timescale presented in this paper) [*Gebhardt et al.*, 2008] (Figure 5b), NE Pacific Core MD02-2496 [*Hendy and Cosma*, 2008] (Figure 5c), NW Pacific Core MD01-2416 (on timescale presented in this paper) [*Gebhardt et al.*, 2008] (Figure 5d), and NE Atlantic Core SU8118 [*Bard et al.*, 2000] (Figure 5e).

be related to the evolution toward modern low-salinity, incompletely utilized surface waters with a lower salinity and higher Si utilization occurring in the modern NE Pacific compared to the NW Pacific (Figures 1a and 1b). Following the YD, where stratification due to sea ice melting has been constrained to the uppermost NW Pacific surface waters, a freshening of (sub)surface waters during the early Holocene [*Sarnthein et al.*, 2004; *Riethdorf et al.*, 2013] indicates a change toward a comparatively weaker stratification of the uppermost water masses associated with a deepening of the winter mixed layer, possibly resulting in an increased relative supply of nutrients. In the NE Pacific, where there has been no sea ice-induced stratification during the YD, the early Holocene warming and freshening (Figures 3a and 3e) led to comparatively stronger stratified upper ocean waters and a reduced Si supply.

6. Discussion

6.1. Implication of Increased Freshwater Input Into the NE Pacific During HS1

The observed minimum in the $\delta^{18}O_{diat}$/local surface $\delta^{18}O_{sw}$ records occurred during times of enhanced ice-rafted debris (IRD) deposition in the open subarctic NE and NW Pacific (Figures 5a, 5b, 5d) and coincides with an IRD peak found in the coastal eastern North Pacific (Figures 1a and 5c) [*Hendy and Cosma*, 2008] as well as with Heinrich Event 1 (H1) in the North Atlantic, which is characterized by high deposition of IRD (Figure 5e) [*Bard et al.*, 2000] associated with the episodic discharge of icebergs from the Laurentide Ice Sheet (LIS) [*Heinrich*, 1988; *Hemming*, 2004].

The coinciding events in the North Atlantic and the North Pacific suggest a close link between the deglacial meltwater histories of the LIS and the CIS. This link might be related to the external forcing of increasing summer insolation (Figure 6g), which could indicate an increased rate of summer melting. Alternatively, processes happening in the North Atlantic during HS1, particularly associated with the weakening/shutdown of the Atlantic Meridional Overturning Circulation (AMOC) (Figure 6f) [*McManus et al.*, 2004], could have triggered rapid climate change in the North Pacific realm via atmospheric and/or oceanic teleconnections, e.g., through sea level rise [*Rohling et al.*, 2004] or oceanic/atmospheric warming [*Clark et al.*, 2007; *Hendy and Cosma*, 2008].

Between 19.0 and 14.5 ka B.P. the eustatic sea level rose about 8–20 m [*Carlson and Clark*, 2012]. Since the Bering Strait was still closed during HS1, oceanic teleconnections from the North Atlantic via the Arctic Ocean can be discarded for the transmission of rapid climate changes. Generally, increasing sea level may have been of importance for the retreat of CIS glaciers, since they had marine grounding lines during times of maximum ice extent [*Mann and Hamilton*, 1995; *Kaufman et al.*, 2011]. However, according to *Alley et al.* [2007], only rapid changes in sea level >10 m could have acted as a forcing factor to synchronize ice sheet retreat, e.g., due to the stabilizing effect of subglacial sedimentation on glacier grounding lines [*Anandakrishnan et al.*, 2007].

It is commonly agreed that atmospheric circulation and air-sea interaction in the Northern Hemisphere are fundamentally influenced by processes happening in the Atlantic and tropical Pacific [*Alexander et al.*, 2002; *Okumura et al.*, 2009]. Some modeling studies suggest an increased advection of warm, salty surface

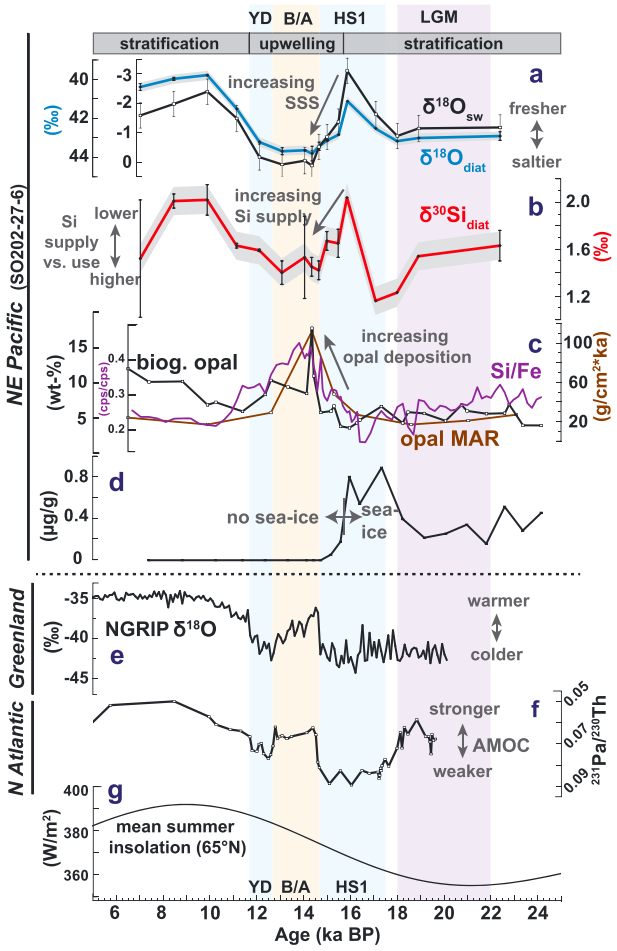

Figure 6. Proxy data from NE Pacific Core SO202-27-6: (a) $\delta^{18}O_{diat}$ and local surface $\delta^{18}O_{sw}$; (b) $\delta^{30}Si_{diat}$; (c) biogenic opal, opal MAR, and Si/Fe ratio; (d) IP_{25} concentration; (e) NGRIP ice core $\delta^{18}O$ record [*North Greenland Ice Core Project* (*NGRIP*) *members*, 2004]; (f) Pa/Th ratio from NW Atlantic Core OCE326-GGC5 [*McManus et al.*, 2004]; and (g) mean summer insolation record at 65°N [*Laskar et al.*, 2004]. Error bars and grey envelopes as delineated in Figure 3.

waters from the subtropical Pacific into the subarctic Pacific in response to the weakening/shutdown of the AMOC [*Kiefer*, 2010; *Okazaki et al.*, 2010]. Such a warming might have accelerated iceberg discharge into the North Pacific [*Hendy and Cosma*, 2008]. However, this hypothesis is not supported by the $\delta^{18}O_{diat}$, $\delta^{18}O_{Nps}$, and SST data (Figures 3a, 3e, and 3g) as well as other (sub)surface temperature/salinity data from the subarctic Pacific [*Max et al.*, 2012; *Riethdorf et al.*, 2013], indicating cold and fresh (sub)surface waters in the NE and NW Pacific during most of HS1. These proxy data are supported by modeling studies arguing for a slight cooling and freshening of the subarctic North Pacific surface waters during HS1 [*Okumura et al.*, 2009] (MIROC model of *Chikamoto et al.* [2012]). Such a cooling could actually have increased Cordilleran Ice Sheet growth, ultimately resulting in enhanced iceberg calving, a scenario similar, even though much smaller scaled, to the scenario proposed for the North Atlantic [*Clark et al.*, 2007]. However, despite smaller, regionally constrained, glacier readvances, the CIS largely retreated during HS1 [*Mann and Peteet*, 1994; *Mann and Hamilton*, 1995]. Furthermore, iceberg calving from the southern CIS into the North Pacific during HS1 seems to have been related to ice retreat, not to ice advance [*Hendy and Cosma*, 2008].

The rapid retreat of the CIS might also have been associated with regional atmospheric warming, which may not be mirrored in the SST records due to a dampening influence of melting ice [*Hendy and Cosma*, 2008]. The change toward higher IP_{25} concentrations at the beginning of HS1 (Figures 6d), which may indicate a switch from a more extensive sea ice cover toward more seasonal sea ice resulting in increased light penetration and IP_{25} production [*Müller et al.*, 2011], supports a dominant atmospheric control if we assume that similar to the Southern Ocean, atmospheric forcing [*Holland and Kwok*, 2012] and local orbital forcing [*WAIS Divide Project Members*, 2013] are mainly controlling sea ice advance and retreat. Furthermore, episodic meltwater outbursts from glacial lakes point toward atmospheric forcing. Ice dam failure repeatedly led to meltwater floods from glacial Lake Missoula, mostly before ~15.6 ka B.P. [*Benito and O'Connor*, 2003; *Hendy*, 2009]. Particularly during the LGM and HS1, when the subarctic front is displaced southward [*Sabin and Pisias*, 1996; *Okumura et al.*, 2009], megaflood events from glacial Lake Missoula might have had the potential to reach the open NE Pacific. Also likely influencing the study site area are megafloods related to the drainage of Alaskan glacial Lake Atna into the NE Pacific, which occurred at least two times between ~26 and 15.5 ka B.P. [*Wiedmer et al.*, 2010]. While most of the freshwater entering the Gulf of Alaska today is transported along the coast within the Alaskan Coastal Current and does not mix offshore [*Weingartner et al.*, 2005], megaflood events likely had a direct impact on the open NE Pacific surface water.

6.2. Late HS1 Paleoceanographic Change in the Subarctic Pacific

A common feature of all SO202-27-6 proxy data presented here is a synchronous change following ~16 ka B.P. (Figures 3a–3g), indicating a prominent paleoceanographic change influencing both surface and subsurface waters, which precedes the paleoclimate change in the North Atlantic realm at the start of the B/A (Figure 6). This late HS1 paleoceanographic change is supported by an increase in *N. seminae* concentration in bulk sediments from the NE Pacific Core MD02-2489 (Figure 3i), which indicate a change toward warmer and comparatively saline surface waters [*Sancetta*, 1982; *Barron et al*., 2009; *Ren et al*., 2014] already in late HS1. Even though the rapid increase in biogenic opal content of NW Pacific Core MD01-2416 at the start of the Bølling seems to support an in-phase behavior with North Atlantic climate (Figure 3m), we suggest that a late HS1 paleoceanographic change represents a true feature of both the NE and the NW Pacific sites, based on two arguments. First, a shift of the observed paleoceanographic change in the Core SO202-27-6 to the HS1-B/A boundary would require a planktic reservoir age of about 1500 years, which is several hundred years higher than previously calculated/assumed reservoir ages for this time slice in the NE Pacific [e.g., *De Vernal and Pederson*, 1997; *Kovanen and Easterbrook*, 2002; *Galbraith et al*., 2008; *Gebhardt et al*., 2008; *Lund et al*., 2011]. Second, pollen data from an independently dated (varve-counted) Japanese Lake Suigetsu sediment core also indicate a paleoclimate change preceding the onset of the Bølling event in the North Atlantic by several hundred years [*Nakagawa et al*., 2003]. We therefore suggest that the HS1-B/A boundary within Core MD01-2416 is located further up core than presented (Figures 3j–3n). This may be possible considering that the HS1-B/A boundary is calculated by linear interpolation between the ^{14}C plateau boundaries. Alternatively, there might be a hiatus of a few centimeters located within the upper part of the ^{14}C plateau.

The observed paleoceanographic change in the subarctic Pacific in late HS1 indicates that a dominant Northern Hemisphere atmospheric control on subarctic Pacific surface water parameters (see section 6.1) has been superimposed by an additional forcing after ~16 ka B.P. In order to explain the late HS1 paleoclimate change recorded in Japanese Lake Suigetsu, *Nakagawa et al*. [2003] proposed a temporal difference between the regional responses of the North Pacific and the North Atlantic climate to changes in solar insolation. A dominant forcing of increasing local summer insolation has also been proposed to explain deglacial Southern Ocean sea ice decline and Antarctic warming [*WAIS Divide Project Members*, 2013]. Related to this, we suggest that a quicker response of the North Pacific region to increasing Northern Hemisphere summer insolation (Figure 6g) relative to the North Atlantic region could have resulted in the observed switch to sea ice-free conditions in the subarctic Pacific already during late HS1 (Figure 6d). The weakened surface water stratification related to the sea ice decline then facilitated an increased input of saline and nutrient-rich deeper waters, stimulating biological productivity prior to the Bølling (Figures 6a–6c). At the start of the Bølling, when the AMOC accelerated (Figure 6f) [*McManus et al*., 2004] and invigorated the influx of southern sourced, nutrient-rich deep waters into the North Pacific [*Galbraith et al*., 2007], upwelling amplified and nutrient supply to the surface waters increased, further promoting productivity (Figures 6a–6c) [*Galbraith et al*., 2007; *Gebhardt et al*., 2008]. This interpretation supports the hypothesis of an increased input of nutrients as primary cause for the peak in export production in the subarctic Pacific realm during the Bølling [*Galbraith et al*., 2007; *Kohfeld and Chase*, 2011] but is in contrast to the study of *Lam et al*. [2013] suggesting transient stratification, possibly associated with meltwater pulse 1a (MWP-1a), as responsible trigger. However, our diatom isotope records do not provide any evidence for freshwater stratification during the time of MWP-1a at 14.6 ka B.P. (Figures 3a and 3b) [*Carlson and Clark*, 2012; *Deschamps et al*., 2012]. Furthermore, since the contribution of the CIS to the eustatic sea level rise of about 14–18 m associated with MWP-1a [*Deschamps et al*., 2012] was probably less than 1 m [*Carlson and Clark*, 2012], freshwater input from the CIS related to MWP-1a was likely restricted to settings influenced by the Alaskan Coastal Current (e.g., Core EW0408-85JC) (Figure 1a) [*Davies et al*., 2011] and did not reach the open NE Pacific.

6.3. Links to Deglacial Rise in Atmospheric pCO_2

Southern Hemisphere processes, including the degassing of CO_2 from the Southern Ocean related to upwelling of CO_2-enriched deep waters during HS1 and the YD [*Skinner et al*., 2010; *Burke and Robinson*, 2012], are generally assumed to have played a dominant role regarding the deglacial rise in atmospheric pCO_2 of ~90 ppm [*Schmitt et al*., 2012; *Parrenin et al*., 2013; *Marcott et al*., 2014]. This view is underlined by

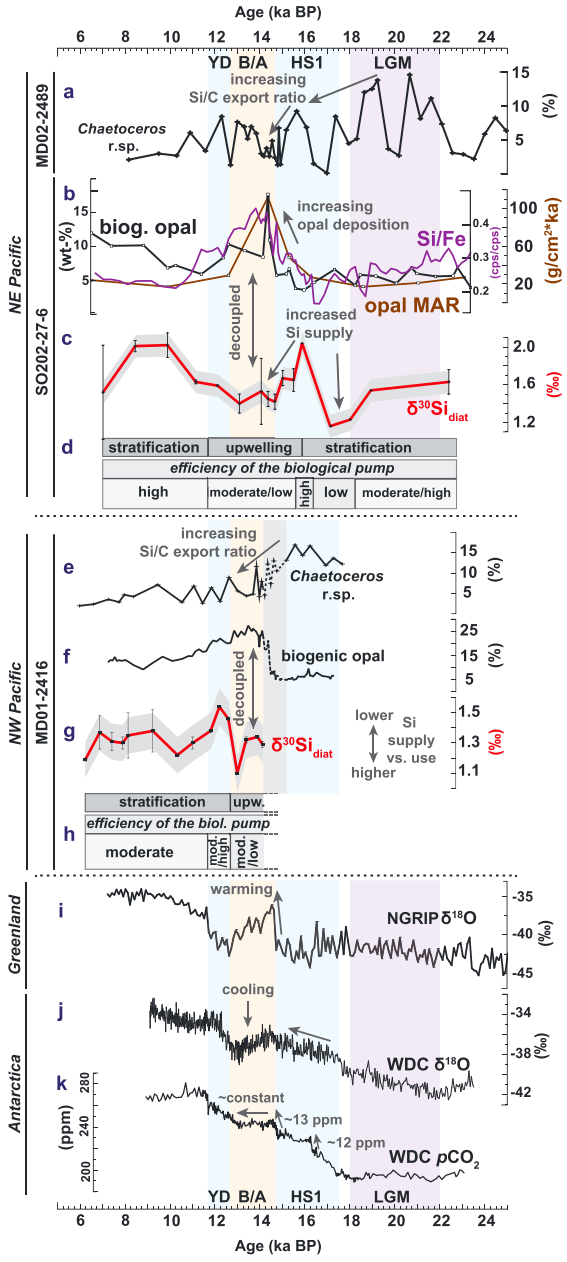

Figure 7. Glacial to Holocene NE and NW Pacific proxy data and interpretation of changes in stratification and the efficiency of the biological pump. (a–d) NE Pacific: Figure 7a shows *Chaetoceros* r. sp. relative abundance from Core MD02-2489 (on timescale presented in this paper). SO202-27-6 (Figures 7b–7d): Figure 7b shows biogenic opal, opal MAR, and Si/Fe ratio. Figure 7c shows $\delta^{30}Si_{diat}$ (error bars and grey envelope as delineated in Figure 3). Figure 7d shows inferred changes in surface water stratification and efficiency of the biological pump. (e–h) NW Pacific Core MD01-2416 (on timescale presented in this paper; grey vertical box as defined in Figure 3): Figure 7e shows *Chaetoceros* r. sp. relative abundance. Figure 7f shows biogenic opal [*Gebhardt et al.*, 2008]. Figure 7g shows $\delta^{30}Si_{diat}$, (error bars indicate errors of replicate analyses). Figure 7h shows inferred changes in surface water stratification and efficiency of the biological pump. (i) NGRIP ice core $\delta^{18}O$ record [*NGRIP members*, 2004], (j) $\delta^{18}O$ from West Antarctic WDC ice core [*WAIS Divide Project Members*, 2013], and (k) atmospheric pCO_2 record from West Antarctic WDC ice core [*Marcott et al.*, 2014].

the close relationship between the atmospheric pCO_2 record and Antarctic temperatures (Figures 7j and 7k). However, recent studies suggest that some CO_2 might have also degassed from the deglacial subarctic Pacific [*Galbraith et al.*, 2007; *Gebhardt et al.*, 2008; *Rae et al.*, 2014], which is characterized by CO_2-rich deep waters. These studies, however, did not yet consider changes in the efficiency of the biological pump, which influences the ocean-atmosphere CO_2 exchange and which can be assessed through changes in nutrient utilization.

Medium-to-high glacial Si utilization in NE Pacific Core SO202-27-6, in combination with increased glacial dust supply [*Lam et al.*, 2013; *Serno et al.*, 2015], is indicative of a moderate-to-highly efficient biological pump (Figures 7c and 7d). The comparatively high relative abundance of *Chaetoceros* r. sp. from nearby Core MD02-2489 (Figure 7a) supports this view, considering that *Chaetoceros* species are weakly silicified diatoms, which indicate a comparatively large export of carbon relative to silica [*Abelmann et al.*, 2006]. An efficient biological pump and stratified NE Pacific surface waters during the last glacial point toward the subarctic Pacific as a sink for CO_2 (Figures 4a and 7d), strengthening the hypothesized link between glacial polar stratification and low atmospheric CO_2 [*Jaccard et al.*, 2005; *Sigman et al.*, 2010]. The increase in Si supply during early HS1 indicates a change toward a regime characterized by a low efficiency of the biological pump (Figures 7c and 7d). Since the enhanced Si supply can be related to enhanced NPIW formation (see section 5.2), which originated in the subarctic Pacific realm [*Max et al.*, 2014] and which was therefore comparatively young and not very enriched in CO_2, we suggest no or only little CO_2 degassing during the early HS1 (Figure 4). This is in contrast to *Rae et al.* [2014], who suggest CO_2 degassing of up to 30 ppm from the subarctic Pacific during that time. However, we think such a scenario unlikely based

on two arguments. First, an amount of 30 ppm would correspond to the about complete rise of atmospheric pCO_2 for that time interval (Figure 7k) and would argue for the subarctic Pacific as main modulator of the atmospheric pCO_2 record. This is considered unlikely given the comparatively small size of the subarctic Pacific and the evidence of Southern Ocean upwelling of CO_2-enriched deep waters during that time [*Skinner et al*., 2010; *Burke and Robinson*, 2012]. Moreover, the CO_2 degassing hypothesis of *Rae et al*. [2014] is linked to increasing SSS in the subarctic Pacific realm. However, the surface water $\delta^{18}O_{sw}$ record does not indicate increasing SSS during early HS1 (Figure 3a), at least not in the NE Pacific realm. At ~16 ka B.P. highest $\delta^{30}Si_{diat}$ then indicate high Si utilization and a highly efficient biological pump (Figures 7c and 7d), suggesting that the subarctic Pacific has been a sink for CO_2 at that time (Figure 4).

The late HS1 increase in upwelling accompanied with an excess Si supply to the photic zone indicates a change toward a comparatively low efficiency of the biological pump, which prevailed during the B/A and possibly also the YD (Figures 7c and 7d). Decoupled $\delta^{30}Si_{diat}$ and opal deposition records in Core MD01-2416 during the B/A (Figures 7f and 7g), as well as the decline in *Chaetoceros* r. sp. particularly in the NW Pacific during late HS1 (Figures 7a and 7e), also indicate a comparatively low efficient biological pump in the NW Pacific (Figure 7h). We therefore suggest that the subarctic Pacific has been a source region of atmospheric CO_2 during late HS1 and the B/A (possibly also the YD in the NE Pacific), actively modulating the atmospheric pCO_2 record (Figure 4). Such a scenario could explain discrepancies between the atmospheric pCO_2 record and Antarctic temperatures particularly during HS1 and the B/A, where abrupt rises in atmospheric CO_2 at ~16.3 ka B.P. (~12 ppm) and over the HS1-B/A transition (~13 ppm) are not mirrored by Antarctic temperatures, and about constant CO_2 levels during the B/A are accompanied by Antarctic cooling (Figures 7j and 7k). *Marcott et al*. [2014] speculated that the atmospheric CO_2 rise at ~16.3 ka B.P. might have been associated with the prominent North Atlantic HS1 iceberg discharge event, which could have eventually triggered a rapid release of terrestrial carbon. Due to the close temporal correlation of this CO_2 rise with the observed subarctic Pacific increase in upwelling and decrease in the efficiency of the biological pump following ~16 ka B.P., one could also argue that the abrupt rise in atmospheric CO_2 at ~16.3 ka B.P. was related to the start of subarctic Pacific CO_2 degassing. Our results of subarctic Pacific CO_2 degassing during late HS1, B/A (and possibly YD in the NE Pacific), are contrary to the hypothesis of *Rae et al*. [2014], who suggest stratified conditions and no CO_2 degassing during late HS1 and the B/A. However, our findings support and further extent the previous studies of *Gebhardt et al*. [2008], who argue for weakened deglacial surface water stratification after ~15 ka B.P., and *Galbraith et al*. [2007], who suggested subarctic Pacific CO_2 degassing over the HS1-B/A transition, related to an increased AMOC.

7. Conclusions

This study presents new combined $\delta^{18}O_{diat}$ and $\delta^{30}Si_{diat}$ records from the subarctic NE Pacific at millennial-scale resolution, for the first time providing data also from the last glacial and early deglacial. Our results show that glacial-to-Holocene changes in the $\delta^{18}O_{diat}$ record are primarily controlled by changes in local surface $\delta^{18}O_{sw}$, demonstrating the potential of $\delta^{18}O_{diat}$ for paleosalinity reconstructions in NE Pacific surface waters. Changes in $\delta^{30}Si_{diat}$, which mirror relative changes in Si utilization, are largely coupled to variations in surface water stratification and associated Si supply. The combined interpretation of both $\delta^{18}O_{diat}$ and $\delta^{30}Si_{diat}$ provides a consistent picture of changes in surface water stratification, Si utilization, and the efficiency of the biological pump, suggesting that the subarctic Pacific was a source region of atmospheric CO_2 during late HS1 and the B/A (possibly also the YD), actively modulating the atmospheric CO_2 record.

Our data reveal an increased freshwater input into the open subarctic NE Pacific, which coincides with H1 IRD event in the North Atlantic, indicating a close link between the CIS and LIS meltwater histories. Future studies should investigate the source, pathway, and extension of the observed freshwater input in the NE Pacific. This is particularly important for general circulation models, which to date do not incorporate meltwater forcing into the North Pacific during HS1. Furthermore, to allow for a more precise evaluation of downcore changes in $\delta^{30}Si_{diat}$, future studies should, e.g., investigate the distribution of silicon isotopes throughout the subarctic Pacific water column and the relationship between the $\delta^{30}Si$ of surface water silicic acid and the $\delta^{30}Si$ of in situ captured diatoms, diatoms from sediment traps, as well as from core tops.

Acknowledgments
The data from this study can be obtained from the PANGAEA database (doi:10.1594/PANGAEA.834308). This study was embedded in the Innovative NOrth Pacific EXperiment (INOPEX), funded by the Bundesministerium für Bildung und Forschung (BMBF). We gratefully acknowledge Michael Sarnthein for providing the additional bulk samples from Core MD01-2416. We thank Ulrike Böttjer, Birgit Glückselig, and Ruth Cordelair for the thorough purification of the diatom material and Gerhard Kuhn for the salt correction of biogenic opal concentration data. Silke Steph is thanked for analyzing *N. pachyderma*$_{sin}$ oxygen and carbon isotopes and Marianne Warnkross for picking *N. pachyderma*$_{sin}$ for radiocarbon dating and isotope analysis. Furthermore, we gratefully acknowledge Philipp Hornung for supporting the error estimation for local surface $\delta^{18}O_{sw}$. Melanie Leng is thanked for providing the lacustrine diatom laboratory standard BFC. Finally, we thank Heiko Pälike and two anonymous reviewers for their constructive comments to improve the manuscript.

References

Abelmann, A., R. Gersonde, G. Cortese, G. Kuhn, and V. Smetacek (2006), Extensive phytoplankton blooms in the Atlantic sector of the glacial Southern Ocean, *Paleoceanography*, *21*, PA1013, doi:10.1029/2005PA001199.

Alexander, M. A., I. Bladé, M. Newman, J. R. Lanzante, N.-C. Lau, and J. D. Scott (2002), The atmospheric bridge: The influence of ENSO teleconnections on air-sea interaction over the global oceans, *J. Clim.*, *15*, 2205–2231.

Allen, J. S., et al. (1983), Physical oceanography of continental shelves, *Rev. Geophys. Space Phys.*, *21*, 1149–1181.

Alley, R. B., S. Anandakrishnan, T. K. Dupont, B. R. Parizek, and D. Pollard (2007), Effect of sedimentation on ice-sheet grounding-line stability, *Science*, *315*, 1838–1841.

Anandakrishnan, S., G. A. Catania, R. B. Alley, and H. J. Horgan (2007), Discovery of till deposition at the grounding line of Whillans Ice Stream, *Science*, *315*, 1835–1838.

Antonov, J. I., D. Seidov, T. P. Boyer, R. A. Locarnini, A. V. Mishonov, H. E. Garcia, O. K. Baranova, M. M. Zweng, and D. R. Johnson (2010), *World Ocean Atlas 2009, Volume 2: Salinity*, U.S. Gov. Print. Off., Washington, D. C.

Ayers, J. M., and M. S. Lozier (2012), Unraveling dynamical controls on the North Pacific carbon sink, *J. Geophys. Res.*, *117*, C01017, doi:10.1029/2011JC007368.

Bard, E., F. Rostek, J.-L. Turon, and S. Gendreau (2000), Hydrological impact of Heinrich events in the subtropical northeast Atlantic, *Science*, *289*, 1321–1324.

Barron, J. A., D. Bukry, W. E. Dean, J. A. Addison, and B. Finney (2009), Paleoceanography of the Gulf of Alaska during the past 15,000 years: Results from diatoms, siliconflagellates, and geochemistry, *Mar. Micropaleontol.*, *72*, 176–195.

Bauch, D., H. Erlenkeuser, G. Winckler, G. Pavlova, and J. Thiede (2002), Carbon isotopes and habitat of polar planktic foraminifera in the Okhotsk Sea: The "carbonate ion effect" under natural conditions, *Mar. Micropaleontol.*, *45*, 83–99.

Belt, S. T., G. Massé, S. J. Rowland, M. Poulin, C. Michel, and B. LeBlanc (2007), A novel chemical fossil of palaeo sea ice: IP_{25}, *Org. Geochem.*, *38*, 16–27.

Benito, G., and J. E. O'Connor (2003), Number and size of last-glacial Missoula floods in the Columbia River valley between the Pasco Basin, Washington, and Portland, Oregon, *Geol. Soc. Am. Bull.*, *115*, 624–638.

Brandriss, M. E., J. R. O'Neill, M. B. Edlund, and E. F. Stoermer (1998), Oxygen isotope fractionation between diatomaceous silica and water, *Geochim. Cosmochim. Acta*, *62*, 1119–1125.

Brewer, T. S., M. J. Leng, A. W. Mackay, A. L. Lamb, J. J. Tyler, and N. G. Marsh (2008), Unravelling contamination signals in biogenic silica oxygen isotope composition: The role of major and trace element geochemistry, *J. Quat. Sci.*, *23*, 321–330.

Broecker, W. S., T.-H. Peng, J. Jouzel, and G. Russell (1990), The magnitude of global fresh-water transports of importance to ocean circulation, *Clim. Dyn.*, *4*, 73–79.

Bronk Ramsey, C., et al. (2012), A complete terrestrial radiocarbon record for 11.2 to 52.8 kyr B.P., *Science*, *338*, 370–374.

Brown, T. A., S. T. Belt, A. Tatarek, and C. J. Mundy (2014), Source identification of the Arctic sea ice proxy IP_{25}, *Nat. Commun.*, *5*, 4197.

Brzezinski, M. A., C. J. Pride, V. M. Franck, D. M. Sigman, J. L. Sarmiento, K. Matsumoto, N. Gruber, G. H. Rau, and K. H. Coale (2002), A switch from $Si(OH)_4$ to NO_3^- depletion in the glacial Southern Ocean, *Geophys. Res. Lett.*, *29*(12), 1564, doi:10.1029/2001GL014349.

Burke, A., and L. F. Robinson (2012), The Southern Ocean's role in carbon exchange during the last deglaciation, *Science*, *335*, 557–561.

Carlson, A. E., and P. U. Clark (2012), Ice sheet sources of sea level rise and freshwater discharge during the last deglaciation, *Rev. Geophys.*, *50*, RG4007, doi:10.1029/2011RG000371.

Chapligin, B., H. Meyer, H. Friedrichsen, A. Marent, E. Sohns, and H.-W. Hubberten (2010), A high-performance, safer and semi-automated approach for the $\delta^{18}O$ analysis of diatom silica and new methods for removing exchangeable oxygen, *Rapid Commun. Mass Spectrom.*, *24*, 2655–2664.

Chapligin, B., et al. (2011), Inter-laboratory comparison of oxygen isotope compositions from biogenic silica, *Geochim. Cosmochim. Acta*, *75*, 7242–7256.

Chapligin, B., H. Meyer, A. Bryan, J. Snyder, and H. Kemnitz (2012), Assessment of purification and contamination correction methods for analysing the oxygen isotope composition from biogenic silica, *Chem. Geol.*, *300–301*, 185–199.

Chikamoto, M. O., L. Menviel, A. Abe-Ouchi, R. Ohgaito, A. Timmermann, Y. Okazaki, N. Harada, A. Oka, and A. Mouchet (2012), Variability in North Pacific intermediate and deep water ventilation during Heinrich events in two coupled climate models, *Deep Sea Res., Part II*, *61*, 114–126.

Clague, J. J., and T. S. James (2002), History and isostatic effects of the last ice sheet in southern British Columbia, *Quat. Sci. Rev.*, *21*, 71–87.

Clark, P. U., S. W. Hostetler, N. G. Pisias, A. Schmittner, and K. J. Meissner (2007), Mechanisms for an ~7-kyr climate and sea-level oscillation during marine isotope stage 3, *Geophys. Monogr. Ser.*, *173*, 209–246.

Craig, H., and L. I. Gordon (1965), Deuterium and oxygen 18 variations in the ocean and the marine atmosphere, in *Stable Isotopes in Oceanographic Studies and Paleotemperatures*, edited by E. Tongiorgi, Consiglio Nazionale delle Ricerche, Spoleto.

Crespin, J., R. Yam, X. Crosta, G. Massé, S. Schmidt, P. Campagne, and A. Shemesh (2014), Holocene glacial discharge fluctuations and recent instability in East Antarctica, *Earth Planet. Sci. Lett.*, *394*, 38–47.

Davies, M. H., A. C. Mix, J. S. Stoner, J. A. Addison, J. Jaeger, B. Finney, and J. Wiest (2011), The deglacial transition on the southeastern Alaska Margin: Meltwater input, sealevel rise, marine productivity, and sedimentary anoxia, *Paleoceanography*, *26*, PA2223, doi:10.1029/2010PA002051.

De la Rocha, C. L., M. A. Brzezinski, and M. J. DeNiro (1997), Fractionation of silicon isotopes by marine diatoms during biogenic silica formation, *Geochim. Cosmochim. Acta*, *61*, 5051–5056.

De la Rocha, C. L., M. A. Brzezinski, M. J. DeNiro, and A. Shemesh (1998), Silicon-isotope composition of diatoms as an indicator of past oceanic change, *Nature*, *395*, 680–683.

De Vernal, A., and T. F. Pederson (1997), Micropaleontology and palynology of core PAR87A-10: A 23,000 year record of paleoenvironmental changes in the Gulf of Alaska, northeast North Pacific, *Paleoceanography*, *12*, 821–830, doi:10.1029/97PA02167.

Deschamps, P., N. Durand, E. Bard, B. Hamelin, G. Camoin, A. L. Thomas, G. M. Henderson, J. I. Okuno, and Y. Yokoyama (2012), Ice-sheet collapse and sea-level rise at the Bølling warming 14,600 years ago, *Nature*, *483*, 559–564.

Ding, T., S. Jiang, D. Wan, Y. Li, J. Li, H. Song, Z. Liu, and X. Yao (1996), *Silicon Isotope Geochemistry*, 1st. ed., 125 pp., Geological House, Beijing.

Dodd, J. P., and Z. D. Sharp (2010), A laser fluorination method for oxygen isotope analysis of biogenic silica and a new oxygen isotope calibration of modern diatoms in freshwater environments, *Geochim. Cosmochim. Acta*, *74*, 1381–1390.

Dodimead, A. J., F. Favorite, and T. Hirano (1963), Salmon of the North Pacific Ocean. Part II, *Bull. Int. North Pacific Fish. Comm.*, *13*, 1–195.

Douthitt, C. B. (1982), The geochemistry of the stable isotopes of silicon, *Geochim. Cosmochim. Acta*, *46*, 1449–1458.

Emile-Geay, J., M. A. Cane, N. Naik, R. Seager, A. C. Clement, and A. van Geen (2003), Warren revisited: Atmospheric freshwater fluxes and "Why is no deepwater formed in the North Pacific", *J. Geophys. Res.*, *108*, 3178, doi:10.1029/2001JC001058.

Galbraith, E. D., S. L. Jaccard, T. F. Pedersen, D. M. Sigman, G. H. Haug, M. Cook, J. R. Southon, and R. Francois (2007), Carbon dioxide release from the North Pacific abyss during the last deglaciation, *Nature*, *449*, 890–894.
Galbraith, E. D., M. Kienast, S. L. Jaccard, T. F. Pederson, B. G. Brunelle, D. M. Sigman, and T. Kiefer (2008), Consistent relationship between global climate and surface nitrate utilization in the western subarctic Pacific throughout the last 500 ka, *Paleoceanography*, *23*, PA2212, doi:10.1029/2007PA001518.
Garcia, H. E., R. A. Locarnini, T. P. Boyer, and J. I. Antonov (2010), *World Ocean Atlas 2009, Volume 4: Nutrients (Phosphate, Nitrate, and Silicate)*, *NOAA Atlas NESDIS 71*, edited by S. Levitus, 398 pp., U.S. Gov. Print. Off., Washington, D. C.
Gebhardt, H., M. Sarnthein, P. M. Grootes, T. Kiefer, H. Kuehn, F. Schmieder, and U. Röhl (2008), Paleonutrient and productivity records from the subarctic North Pacific for Pleistocene glacial terminations I to V, *Paleoceanography*, *23*, PA4212, doi:10.1029/2007PA001513.
Gersonde, R., and SO202-INOPEX Participants (2010), Cruise report of the SO202-INOPEX cruise, 181 pp.
Gersonde, R., and U. Zielinski (2000), The reconstruction of late Quaternary Antarctic sea ice distribution—The use of diatoms as a proxy for sea ice, *Palaeogeogr. Palaeoclimatol. Palaeoecol.*, *162*, 263–286.
Harrison, P. J., P. W. Boyd, D. E. Varela, S. Takeda, A. Shiomoto, and T. Odate (1999), Comparison of factors controlling phytoplankton productivity in the NE and NW subarctic Pacific gyres, *Prog. Oceanogr.*, *43*, 205–234.
Heinrich, H. (1988), Origin and consequences of cyclic ice rafting in the northeast Atlantic Ocean during the past 130,000 years, *Quat. Res.*, *29*, 142–152.
Hemming, S. R. (2004), Heinrich events: Massive late Pleistocene detritus layers of the North Atlantic and their global climate imprint, *Rev. Geophys.*, *42*, RG1005, doi:10.1029/2003RG000128.
Hendry, K. R., and L. F. Robinson (2012), The relationship between silicon isotope fractionation in sponges and silicic acid concentration: Modern and core-top studies of biogenic opal, *Geochim. Cosmochim. Acta*, *81*, 1–12.
Hendry, K. R., and M. A. Brzezinski (2014), Using silicon isotopes to understand the role of the Southern Ocean in modern and ancient biogeochemistry and climate, *Quat. Sci. Rev.*, *89*, 13–26.
Hendy, I. (2009), A fresh perspective on the Cordilleran Ice Sheet, *Geology*, *37*, 95–96.
Hendy, I. L., and T. Cosma (2008), Vulnerability of the Cordilleran Ice Sheet to iceberg calving during late Quaternary rapid climate change events, *Paleoceanography*, *23*, PA2101, doi:10.1029/2008PA001606.
Holland, P. R., and R. Kwok (2012), Wind-driven trends in Antarctic sea-ice drift, *Nat. Geosci.*, *5*, 872–875.
Jaccard, S. L. (2012), Palaeoceanography: Pacific and Atlantic synchronized, *Nat. Geosci.*, *5*, 594–596.
Jaccard, S. L., and E. D. Galbraith (2013), Direct ventilation of the North Pacific did not reach the deep ocean during the last deglaciation, *Geophys. Res. Lett.*, *40*, 199–203, doi:10.1029/2012GL054118.
Jaccard, S. L., G. H. Haug, D. M. Sigman, T. F. Pedersen, H. R. Thierstein, and U. Röhl (2005), Glacial/interglacial changes in subarctic North Pacific stratification, *Science*, *308*, 1003–1006.
Juillet-Leclerc, A., and L. Labeyrie (1987), Temperature dependance of the oxygen isotopic fractionation between diatom silica and water, *Earth Planet. Sci. Lett.*, *84*, 69–74.
Kaufman, D. S., N. E. Young, J. P. Briner, and W. F. Manley (2011), Alaska Palaeo-Glacier Atlas (version 2), *Dev. Quat. Sci.*, *15*, 427–445.
Kiefer, T. (2010), When still waters ran deep, *Science*, *329*, 290–291.
Kohfeld, K. E., and Z. Chase (2011), Controls on deglacial changes in biogenic fluxes in the North Pacific Ocean, *Quat. Sci. Rev.*, *30*, 3350–3363.
Kovanen, D. J., and D. J. Easterbrook (2002), Paleodeviations of radiocarbon marine reservoir values for the northeast Pacific, *Geology*, *30*, 243–246.
Kuhn, G. (2013), Don't forget the salty soup: Calculations for bulk marine geochemistry and radionuclide geochronology, Goldschmidt 2013 Conference Abstracts, Florence, Mineralogical Magazine.
Lam, P. J., L. F. Robinson, J. Blusztajn, C. Li, M. S. Cook, J. F. McManus, and L. D. Keigwin (2013), Transient stratification as the cause of the North Pacific productivity spike during deglaciation, *Nat. Geosci.*, doi:10.1038/NGEO1873.
Laskar, J., P. Robutel, F. Joutel, M. Gastineau, A. C. M. Correia, and B. Levrard (2004), A long-term numerical solution for the insolation quantities of the Earth, *Astron. Astrophys.*, *428*, 261–285.
Lefèvre, N., A. J. Watson, D. J. Cooper, R. F. Weiss, T. Takahashi, and S. C. Sutherland (1999), Assessing the seasonality of the oceanic sink for CO_2 in the northern hemisphere, *Global Biogeochem. Cycles*, *13*, 273–286, doi:10.1029/1999GB900001.
Lund, D. C., A. C. Mix, and J. Southon (2011), Increased ventilation age of the deep northeast Pacific Ocean during the last deglaciation, *Nat. Geosci.*, *4*, 771–774.
Maier, E., B. Chapligin, A. Abelmann, R. Gersonde, O. Esper, J. Ren, H. Friedrichsen, H. Meyer, and R. Tiedemann (2013), Combined oxygen and silicon isotope analysis of diatom silica from a deglacial subarctic Pacific record, *J. Quat. Sci.*, *28*, 571–581.
Mann, D. H., and D. M. Peteet (1994), Extent and timing of the Last Glacial Maximum in Southwestern Alaska, *Quat. Res.*, *42*, 136–148.
Mann, D. H., and T. D. Hamilton (1995), Late Pleistocene and Holocene paleoenvironments of the North Pacific coast, *Quat. Sci. Rev.*, *14*, 449–471.
Marchetti, A., P. Juneau, F. A. Whitney, C.-S. Wong, and P. J. Harrison (2006), Phytoplankton processes during a mesoscale iron enrichment in the NE subarctic Pacific: Part II—Nutrient utilization, *Deep Sea Res., Part II*, *53*, 2114–2130.
Marcott, S. A., et al. (2014), Centennial-scale changes in the global carbon cycle during the last deglaciation, *Nature*, *514*, 616–619.
Max, L., J.-R. Riethdorf, R. Tiedemann, M. Smirnova, L. Lembke-Jene, K. Fahl, D. Nürnberg, A. Matul, and G. Mollenhauer (2012), Sea surface temperature variability and sea-ice extent in the subarctic northwest Pacific during the past 15,000 years, *Paleoceanography*, *27*, PA3213, doi:10.1029/2012PA002.
Max, L., L. Lembke-Jene, J.-R. Riethdorf, R. Tiedemann, D. Nürnberg, H. Kühn, and A. Mackensen (2014), Pulses of enhanced North Pacific Intermediate Water ventilation from the Okhotsk Sea and Bering Sea during the last deglaciation, *Clim. Past*, *10*, 591–605.
McManus, J. F., R. Francois, J. M. Gherardi, L. D. Keigwin, and S. Brown-Leger (2004), Collapse and rapid resumption of Atlantic meridional circulation linked to deglacial climate changes, *Nature*, *428*, 834–837.
Méheust, M., K. Fahl, and R. Stein (2013), Variability in modern sea surface temperature, sea ice and terrigenous input in the sub-polar North Pacific and Bering Sea: Reconstruction from biomarker dara, *Org. Geochem.*, *57*, 54–64.
Meredith, M. P., M. A. Brandon, M. I. Wallace, A. Clarke, M. J. Leng, I. A. Renfrew, N. P. M. van Lipzig, and J. C. King (2008), Variability in the freshwater balance of northern Marguerite Bay, Antarctic Peninsula: Results from $\delta^{18}O$, *Deep Sea Res., Part II*, *55*, 309–322.
Milligan, A. J., D. E. Varela, M. A. Brzezinski, and F. M. M. Morel (2004), Dynamics of silicon metabolism and silicon isotopic discrimination in a marine diatom as a function of pCO_2, *Limnol. Oceanogr.*, *49*, 322–329.
Mulitza, S., D. Boltovskoy, B. Donner, H. Meggers, A. Paul, and G. Wefer (2003), Temperature: $\delta^{18}O$ relationships of planktonic foraminifera collected from surface waters, *Palaeogeogr. Palaeoclimatol. Palaeoecol.*, *202*, 143–152.
Müller, J., A. Wagner, K. Fahl, R. Stein, M. Prange, and G. Lohmann (2011), Towards quantitative sea ice reconstructions in the northern North Atlantic: A combined biomarker and numerical modelling approach, *Earth Planet. Sci. Lett.*, *306*, 137–148.

Müller, P. J., and R. Schneider (1993), An automated leaching method for the determination of opal in sediments and particulate matter, *Deep Sea Res., Part I*, *40*, 425–444.
Nakagawa, T., H. Kitagawa, Y. Yasuda, P. Tarasov, K. Nishida, K. Gotanda, Y. Sawai, and Y. R. C. P. Members (2003), Asynchronous climate changes in the North Atlantic and Japan during the Last Termination, *Science*, *299*, 688–691.
North Greenland Ice Core Project Members (2004), High-resolution record of Northern Hemisphere climate extending into the last interglacial period, *Nature*, *431*, 147–151.
Okazaki, Y., A. Timmermann, L. Menviel, N. Harada, A. Abe-Ouchi, M. O. Chikamoto, A. Mouchet, and H. Asahi (2010), Deepwater formation in the North Pacific during the Last Glacial Termination, *Science*, *329*, 200–204.
Okumura, Y. M., C. Deser, A. Hu, A. Timmermann, and S.-P. Xie (2009), North Pacific climate response to freshwater forcing in the subarctic North Atlantic: Oceanic and atmospheric pathways, *J. Clim.*, *22*, 1424–1444.
Onodera, J., K. Takahashi, and M. C. Honda (2005), Pelagic and coastal diatom fluxes and the environmental changes in the northwestern North Pacific during December 1997–May 2000, *Deep Sea Res., Part II*, *52*, 2218–2239.
Parrenin, F., V. Masson-Delmotte, P. Köhler, D. Raynaud, D. Paillard, J. Schwander, C. Barbante, A. Landais, A. Wegner, and J. Jouzel (2013), Synchronous change of atmospheric CO_2 and Antarctic temperature during the last deglacial warming, *Science*, *339*, 1060–1063.
Rae, J. W. B., M. Sarnthein, G. L. Foster, A. Ridgwell, P. M. Grootes, and T. Elliott (2014), Deep water formation in the North Pacific and deglacial CO_2 rise, *Paleoceanography*, *29*, 645–667, doi:10.1002/2013PA002570.
Reimer, P. J., et al. (2013), INTCAL13 and MARINE13 radiocarbon age calibration curves 0–50,000 years cal BP, *Radiocarbon*, *55*, 1869–1887.
Ren, J., R. Gersonde, O. Esper, and C. Sancetta (2014), Diatom distribution in northern North Pacific surface sediments and their relationship to modern environmental variables, *Palaeogeogr. Palaeoclimatol. Palaeoecol.*, *402*, 81–103.
Reynolds, B. C., M. Frank, and A. N. Halliday (2006), Silicon isotope fractionation during nutrient utilization in the North Pacific, *Earth Planet. Sci. Lett.*, *244*, 431–443.
Reynolds, B. C., M. Frank, and A. N. Halliday (2008), Evidence for a major change in silicon cycling in the sucarctic North Pacific a 2.73 Ma, *Paleoceanography*, *23*, PA4219, doi:10.1029/2007PA001563.
Riethdorf, J.-R., L. Max, D. Nürnberg, L. Lembke-Jene, and R. Tiedemann (2013), Deglacial development of (sub) sea surface temperature and salinity in the subarctic northwest Pacific: Implications for upper-ocean stratification, *Paleoceanography*, *28*, 91–104, doi:10.1002/palo.20014.
Rohling, E. J., R. Marsh, N. C. Wells, M. Siddall, and N. R. Edwards (2004), Similar meltwater contributions to glacial sea level changes from Antarctic and northern ice sheets, *Nature*, *430*, 1016–1021.
Sabin, A. L., and N. G. Pisias (1996), Sea surface temperature changes in the northeastern Pacific Ocean during the Past 20,000 years and their relationship to climate change in northwestern North America, *Quat. Res.*, *46*, 48–61.
Sancetta, C. (1982), Distribution of diatom species in surface sediments of the Bering and Okhotsk seas, *Micropaleontology*, *28*, 221–257.
Sancetta, C. (1987), Three species of *Coscinodiscus* Ehrenberg from North Pacific sediments examined in the light and scanning electron microscopes, *Micropaleontology*, *33*, 230–241.
Sarmiento, J. L., N. Gruber, M. A. Brzezinski, and J. P. Dunne (2004), High-latitude controls of thermocline nutrients and low latitude biological productivity, *Nature*, *427*, 56–60.
Sarnthein, M., H. Gebhardt, T. Kiefer, M. Kucera, M. Cook, and H. Erlenkeuser (2004), Mid Holocene origin of the sea-surface salinity low in the subarctic North Pacific, *Quat. Sci. Rev.*, *23*, 2089–2099.
Sarnthein, M., P. M. Grootes, J. P. Kennett, and M.-J. Nadeau (2007), ^{14}C reservoir ages show deglacial changes in ocean currents and carbon cycle, *Geophys. Monogr. Ser.*, *173*, 175–196.
Sarntheim, M., B. Schneider, and P. M. Grootes (2015), Peak glacial ^{14}C ventilation ages suggest major drawdown of carbon into the abyssal ocean, *Clim. Past*, *9*, 2595–2614.
Schmidt, M., R. Botz, D. Rickert, G. Bohrmann, S. R. Hall, and S. Mann (2001), Oxygen isotopes in marine diatoms and relations to opal-A maturation, *Geochim. Cosmochim. Acta*, *65*, 201–211.
Schmitt, J., et al. (2012), Carbon isotope constraints on the deglacial CO_2 rise from ice cores, *Science*, *336*, 711–714.
Schrader, H. J., and R. Gersonde (1978), Diatoms and silicoflagellates, *Utrecht Micropaleontol. Bull.*, *17*, 129–176.
Serno, S., G. Winckler, R. F. Anderson, E. Maier, H. Ren, R. Gersonde, and G. H. Haug (2015), Comparing dust flux records from the Subarctic North Pacific and Greenland: Implications for atmospheric transport to Greenland and for the application of dust as a chronostratigraphic tool, *Paleoceanography*, *30*, doi:10.1002/2014PA002748.
Shcherbina, A. Y., L. D. Talley, and D. L. Rudnick (2003), Direct observations of North Pacific ventilation: Brine rejection in the Okhotsk Sea, *Science*, *302*, 1952–1955.
Shemesh, A., L. H. Burckle, and J. D. Hays (1994), Meltwater input to the Southern Ocean during the Last Glacial Maximum, *Science*, *266*, 1542–1544.
Shemesh, A., D. Hodell, X. Crosta, S. Kanfoush, C. Charles, and T. Guilderson (2002), Sequence of events during the last deglaciation in Southern Ocean sediments and Antarctic ice cores, *Paleoceanography*, *17*(4), 1056, doi:10.1029/2000PA000599.
Sheppard, A. M. F., and H. A. Gilg (1996), Stable isotope geochemistry of clay minerals, *Clay Miner.*, *31*, 1–24.
Shimizu, Y., T. Iwao, I. Yasuda, S.-I. Ito, T. Watanabe, K. Uehara, N. Shikama, and T. Nakano (2004), Formation process of North Pacific Intermediate Water revealed by profiling floats set to drift on 26.7σ_θ isopycnal surface, *J. Oceanogr.*, *60*, 453–462.
Sigman, D. M., M. P. Hain, and G. H. Haug (2010), The polar ocean and glacial cycles in atmospheric CO_2 concentration, *Nature*, *466*, 47–55.
Sikes, E. L., J. K. Volkman, L. G. Robertson, and J.-J. Pichon (1997), Alkenones and alkenes in surface waters and sediments of the Southern Ocean: Implications for paleotemperature estimation in polar regions, *Geochim. Cosmochim. Acta*, *61*, 1495–1505.
Skinner, L. C., S. Fallon, C. Waelbroeck, and S. Barker (2010), Ventilation of the deep Southern Ocean and deglacial CO_2 rise, *Science*, *328*, 1147–1151.
Stabeno, P. J., N. A. Bond, A. J. Hermann, N. B. Kachel, C. W. Mordy, and J. E. Overland (2004), Meteorology and oceanography of the Northern Gulf of Alaska, *Cont. Shelf Res.*, *24*, 859–897.
Stoynova, V., T. M. Shanahan, K. A. Hughen, and A. de Vernal (2013), Insights into circum-Arctic sea ice variability from molecular geochemistry, *Quat. Sci. Rev.*, *79*, 63–73.
Stuiver, M., and P. J. Reimer (1993), Extended ^{14}C data base and revised CALIB 3.0 ^{14}C age calibration program, *Radiocarbon*, *35*, 215–230.
Sun, X., M. Olofsson, P. S. Andersson, B. Fry, C. Legrand, C. Humborg, and C.-M. Mörth (2014), Effects of growth and dissolution on the fractionation of silicon isotopes by estuarine diatoms, *Geochim. Cosmochim. Acta*, *130*, 156–166.
Sutton, J. N., D. E. Varela, M. A. Brzezinski, and C. P. Beucher (2013), Species-dependent silicon isotope fractionation by marine diatoms, *Geochim. Cosmochim. Acta*, *104*, 300–309.
Swann, G. E. A., and M. J. Leng (2009), A review of diatom $\delta^{18}O$ in palaeoceanography, *Quat. Sci. Rev.*, *28*, 384–398.
Takahashi, K. (1986), Seasonal fluxes of pelagic diatoms in the subarctic Pacific, 1982–1983, *Deep Sea Res.*, *33*, 1225–1251.

Takahashi, K., J. D. Billings, and J. K. Morgan (1990), Oceanic provinces: Assessment from the time-series diatom fluxes in the northeastern Pacific, *Limnol. Oceanogr.*, *35*, 154–165.
Takeda, S. (1998), Influence of iron variability on nutrient consumption ratio of diatoms in oceanic waters, *Nature*, *393*, 774–777.
Takeda, S. (2011), Iron and phytoplankton growth in the subarctic North Pacific, *Aqua-BioScience Monogr.*, *4*, 41–93.
Takeda, S., and A. Tsuda (2005), An in situ iron-enrichment experiment in the western subarctic Pacific (SEEDS): Introduction and summary, *Prog. Oceanogr.*, *64*, 95–109.
Taylor, H. P. J. (1968), The oxygen isotope geochemistry of igneous rocks, *Contrib. Mineral. Petrol.*, *19*, 1–71.
Tsuda, A., et al. (2007), Evidence for the grazing hypothesis: Grazing reduces phytoplankton responses of the HNLC ecosystem to iron enrichment in the western subarctic Pacific (SEEDS II), *J. Oceanogr.*, *63*, 983–994.
Waelbroeck, C., L. Labeyrie, E. Michel, J. C. Duplessy, J. F. McManus, K. Lambeck, E. Balbon, and M. Labracherie (2002), Sea-level and deep water temperature changes derived from benthic foraminifera isotopic records, *Quat. Sci. Rev.*, *21*, 295–305.
WAIS Divide Project Members (2013), Onset of deglacial warming in West Antarctica driven by local orbital forcing, *Nature*, *500*, 440–444.
Warren, B. A. (1983), Why is no deep water formed in the North Pacific?, *J. Mar. Res.*, *41*, 327–347.
Weingartner, T. J., S. L. Danielson, and T. C. Royer (2005), Freshwater variability and predictability in the Alaska Costal Current, *Deep Sea Res., Part II*, *52*, 169–191.
Wiedmer, M., D. R. Montgomery, A. R. Gillespie, and H. Greenberg (2010), Late Quaternary megafloods from Glacial Lake Atna, Couthcentral Alaska, U.S.A., *Quat. Res.*, *73*, 413–424.
Yasuda, I. (1997), The origin of the North Pacific Intermediate Water, *J. Geophys. Res.*, *102*, 893–909, doi:10.1029/96JC02938.
You, Y. (2003), The pathway and circulation of North Pacific Intermediate Water, *Geophys. Res. Lett.*, *30*(24), 2291, doi:10.1029/2003GL018561.
Ziegler, K., O. A. Chadwick, M. A. Brzezinski, and E. F. Kelly (2005), Natural variations of δ^{30}Si ratios during progressive basalt weathering, Hawaiian Islands, *Geochim. Cosmochim. Acta*, *69*, 4597–4610.

Erratum

In the originally published version of this article, Figures 3 and 6 were published incorrectly. This has since been corrected and this version may be considered the authoritative version of record.